Durham University

Durham Research Online

Deposited in DRO:

26 June 2014

Version of attached file:

Accepted Version

Peer-review status of attached file:

Peer-reviewed

Citation for published item:

Christopher, T. and Humphreys, M.C.S. and Barclay, J. and Genareau, K. and De Angelis, S.M.H. and Plail, M. and Donovan, A. (2014) 'Petrological and geochemical variation during the Soufrière Hills eruption, 1995 to 2010.', Memoirs., 39 . pp. 317-342.

Further information on publisher's website:

http://dx.doi.org/10.1144/M39.17

Publisher's copyright statement:

© Geological Society of London 2014

Additional information:

The Eruption of Soufrière Hills Volcano, Montserrat from 2000 to 2010. Chapter 17.

Use policy

The full-text may be used and/or reproduced, and given to third parties in any format or medium, without prior permission or charge, for personal research or study, educational, or not-for-profit purposes provided that:

- a full bibliographic reference is made to the original source
- a link is made to the metadata record in DRO
- the full-text is not changed in any way

The full-text must not be sold in any format or medium without the formal permission of the copyright holders.

Please consult the full DRO policy for further details.

Durham University Library, Stockton Road, Durham DH1 3LY, United Kingdom
Tel : +44 (0)191 334 3042 | Fax : +44 (0)191 334 2971
https://dro.dur.ac.uk

Petrological and Geochemical Variation during the Soufrière Hills Eruption (1995-2010)

Thomas E. Christopher [1]*, Madeleine C. S. Humphreys [2,3], Jenni Barclay [4], Kimberly Genareau [5], Sarah M.H. De Angelis [6], Melissa Plail [4], Amy Donovan [7]

1 Montserrat Volcano Observatory, Salem, Montserrat, West Indies.

2 Earth Sciences Department, University of Oxford, South Parks Road, Oxford OX1 3AN, UK.

3 Present address: Department of Earth Sciences, Durham University, Science Labs, Durham, DH1 3LE, UK

4 School of Environmental Sciences, University of East Anglia, Norwich NR9 7TJ, UK.

5 Department of Earth and Environmental Sciences, Lehigh University, 1 West Packer Avenue Bethlehem, PA 18015-3001 USA

6 Geophysical Institute, University of Alaska Fairbanks, 903 Koyukuk Drive, P.O. Box 757320, Fairbanks, AK

7 Department of Geography, University of Cambridge, Downing Place, Cambridge CB2 3EN

*corresponding author; Thomas@mvo.ms

Words = 11744 References = 101 Tables = 16 Figures = 11

Abbreviated Title: Petrological and Geochemical variation

ABSTRACT

The andesite lava erupted at the Soufrière Hills Volcano is crystal rich with 33-63% phenocrysts, of plagioclase (65%); amphibole (28%), orthopyroxene (7%) and minor Fe-Ti oxide and clinopyroxene microphenocrysts. The andesite hosts mafic enclaves which have similar mineral phases to the andesite. The enclaves are generally crystal poor but can have up to 27% of inherited phenocrysts from the andesite, the majority of which are plagioclase. The eruption is defined by discrete periods of extrusion called phases, separated by pauses. The enclaves exhibit bulk geochemical trends that are consistent with fractionation. We infer that the intruded mafic liquids of Phases I and II interacted and assimilated plutonic residue remaining from the multiple prior mafic intrusions, while the basaltic liquids from Phases III and V assimilated relatively little material. We also infer a change in the basaltic composition coming from depth. The bulk Fe contents of both magma types are coupled and they both show a systematic inter-phase variation in Fe content. We interpret the coupled Fe variation to be due to contamination of the andesite from the intruding basalt via diffusion and advection processes, resulting in the erupted andesite products bearing the geochemical imprint of the syn-eruptive enclaves.

The Soufrière Hills volcano is an andesitic dome complex located on the island of Montserrat in the Lesser Antilles arc. The present eruption began on the evening of July 18th 1995 with ash venting followed by phreatic explosions over the next weeks and months (Young et al., 1998; Robertson et al., 2000). Juvenile material arrived at the surface around November 15th 1995 (Young et al., 1998) building the first lava dome of the eruption. Lava extrusion and dome growth at Soufrière Hills volcano has not been continuous during the eruption; dome growth has been defined by distinct periods of extrusion referred to as ‘phases’ separated by periods of no activity, referred to as ‘pauses’. Each period of extrusion was volcanologicaly unique, however each of the effusive phases were punctuated by pyroclastic flows generated by dome collapse or Vulcanian explosions.

Phase I of dome growth (mid November 1995 to mid March 1998) was characterized by cyclic growth and frequent collapse of the lava dome, with a mean extrusion rate of 4.5 $m^3 s^{-1}$ (Wadge et al., 2010) which peaked at about 10 $m^3 s^{-1}$ (Herd et al., 2005). The volcanic activity of Phase I is described in detail elsewhere (e.g. Aspinall et al., 1998; Young et al., 1998; Miller et al., 1998; Calder et al., 2002; Norton et al., 2002). The cessation of lava extrusion in March 1998 occurred when a dome with a volume of 113 x 10^6 m^3 was present in the crater (Norton et al., 2002).

Phase II (mid November 1999 to mid July 2003), showed a less variable extrusion rate with a mean of 2.9 $m^3 s^{-1}$ (Wadge et al., 2010), peaking at about 4 $m^3 s^{-1}$ (Herd et al., 2005). This resulted in the construction of a larger volume dome than any extruded during Phase I. Dome collapses were less frequent than during Phase I but involved larger volumes, culminating in the largest volume collapse of the eruption to date in July 2003.This removed almost the entire volume of the dome (~200 x10^6 m^3 Edmonds et al., 2006). The ensuing period of pause lasted 24 months, four months longer than the first pause and to date is the only prolonged period of the eruption with a relatively dome-free crater.

Phase III (early August 2005 to early April 2007), started slowly and the growth rate for most of August was slow and steady (0.5-0.7 m^3/s). Low extrusion rates continued through December and January (3.2-3.9 m^3/s), but the extrusion rate exceeded 10 $m^3 s^{-1}$ in February 2006 and remained high for the rest of the extrusive episode. The dome collapse event on the morning of May 20th 2006 involved ~ 100 x10^6 m^3 of dome material and emptied the crater; however an observation flight later that day revealed new extrusion in the vent area. Subsequent growth continued until extrusive activity stopped in April 2007 leaving a dome of ~ 200 x10^6 m^3 in the crater. This was the largest dome present during any pause for the current eruption. Phase III was characterized by much less pyroclastic flow activity; to such an extent that the first flow large enough to reach the sea occurred on the morning of May 20th 2006.

72

73

74

75 *Phases IV and V volcanic activity*

76 The first three phases of extrusion were characterized by extended periods (on the order of years) of lava
77 production separated by pauses of similar lengths. This was not the case for Phases IV and V. Phase IV
78 was characterized by two separate episodes of extrusion punctuated by explosions, the first episode was in
79 July-August 2008 and the second in December 2008-January 2009. The first episode of Phase IV started
80 with a Vulcanian explosion on July 28th 2008 while the December 2008- January 2009 episode started and
81 ended with Vulcanian explosions on December 3rd 2008 and Jan 3rd 2009 respectively. An approximate
82 volume of 39 x10^{6} m^{3} of andesite was extruded for Phase IV (Wadge et al., 2010). Phase V was also short
83 lived (early October 2009 till mid February 2010), and extruded ~ 74 x10^{6} m^{3}. As was the case with Phase
84 IV, Phase V produced a high occurrence of explosive activity (Stinton et al., this volume). The extrusion
85 was also cyclic and the cycles were characterized by periods of intense pyroclastic flow generation which
86 would wax and wane on time scales ranging from 4 to 13 hours (Odbert et al., this volume). The textures
87 present in the Phase IV and Phase V products are similar to that noticed in Phases I, II and III. There
88 however seems to be an increase in the vesicularity of the andesite products with friable hand specimens
89 being more commonplace in Phases IV and V. The presence of banded pumice in the July 28th 2008
90 explosion products was a new occurrence in the eruption.

91

92 *Aim of Current Work*

93 The initial extrusive episode, Phase I received considerable attention with regards to the petrological and
94 geochemical characteristics of the eruptive products (e.g. Barclay et al., 1998; Devine et al., 1998a;
95 1998b; Murphy et al., 1998; Murphy et al., 2000; Higgins & Roberge, 2003; Zellmer et al., 2003a;
96 2003b). The initial research was focused on constraining pre-eruptive storage conditions of the erupted

andesite (e.g. Barclay et al., 1998; Couch et al., 2003a; Rutherford & Devine, 2003) as well as establishing the role of the intruding mafic magma in the onset and fueling of the eruption (e.g. Murphy et al., 1998; Murphy et al., 2000; Devine et al., 2003). Long lived eruptions (such as the eruption at Arenal volcano, Reagan et al., 1987) can produce products with temporal variations in chemistry and mineralogy, which may provide useful data for unlocking processes responsible for driving such eruptions (e.g. Streck et al., 2002; Bolge et al., 2006; Ryder et al., 2006).

The preliminary research has without doubt provided valuable information about the processes responsible for triggering and driving the eruption and hence influencing the eruption style. However the ongoing nature of the eruption now provides an opportunity to address any temporal variations in textures and chemistry of the minerals as well as the bulk rock compositions that may have occurred as the eruption proceeded. The aim of this publication is to present a holistic overview of geochemical and petrological data collected from the enclaves and host andesite throughout the current Soufrière Hills eruption. The Phase IV and Phase V products are compared to the earlier products, highlighting any temporal variations present and their bearing on magma chamber and eruption processes. In particular, we focus on temporal variations in bulk rock FeO, and propose that this is linked to similar compositional variations in some mineral phases. We also make a brief comparison to the Mt Pelée products where the processes responsible for generating the andesitic compositions are well constrained (e.g. Dupuy et al., 1985; Fichaut et al., 1989a; Pichavant et al., 2002).

ANALYTICAL TECHNIQUES

Microprobe Analysis

Samples from Phase IV were analyzed using a Cameca 5-spectrometer SX-100 instrument at the Department of Earth Sciences University of Cambridge. Minerals were analyzed using a 2 μm, 15 kV, 10

nA beam for major elements and a 100 nA beam for minor and trace elements. Glasses were analyzed using a 10 μm, 15 kV, 2 nA beam to avoid alkali migration (Devine et al., 1995; Humphreys et al., 2006), with a 10 nA beam for minor and trace elements (e.g. Cl, Ti, Mg).

The Phase V minerals were probed using a JEOL8600 four spectrometer instrument at the Research Laboratory for Archaeology & the History of Art, University of Oxford. Minerals were analyzed with a 15 keV, 15 nA, 1 micron beam. Peak analysis count times were 30s, except for Na (20s) and Cl (40s). Glass analysis was carried out with a 15 keV, 6 nA, 10 μm diameter beam. Peak count times for all elements were 30s, except for Na (10s), Cl (40s) and P (60s). Amphibole structural formulae were recalculated on the basis of 23 O atoms following Schumacher (1997) and oxide minerals using Stormer (1983).

Bulk Rock Analysis

Andesite and enclave XRF data from Phase II along with some Phase III andesites were obtained by the MVO with the analyses performed at the University of Leicester labs under MVO contract. This is the same laboratory that produced the Phase I data presented in Murphy et al. (2000) and Zellmer et al. (2003a). The remaining andesite bulk rock data from Phase III and all of Phases IV and V were obtained from the University of East Anglia under MVO contract. Enclave bulk rock data from Phase III onwards was also obtained from the University of East Anglia under MVO contract. Bulk enclave data from Phase II were from two sources, the first being McGill University in Canada and the second from the British Geological Survey (BGS) labs in Nottingham England. Detailed information about lab, instrumentation and samples analyzed by each lab is presented in Table 1. Bulk rock data is unavailable for Phase IV enclaves due to the limited volume of observed basaltic material (mm size inclusions) extruded and the lack of extensive deposits available for sampling. Microprobe glass and mineral chemistry data were however obtained from mafic fragments in some thin sections.

PREVIOUS WORK

Andesite and enclave bulk rock XRF analyses of Phase I major and trace elements were compiled from the literature (Devine et al., 1998a; Murphy et al., 1998; Murphy et al., 2000; Zellmer et al., 2003a). Previous petrological studies on the eruption products of Phases I, II and III, are present in a variety of sources including Barclay et al. (1998), Devine et al. (1998b), Murphy et al. (2000), Couch et al. (2003a; 2003b), Zellmer et al. (2003a), Humphreys et al. (2009a; 2009b), Barclay et al. (2010) Humphreys et al. (2010). Here we summarize the Phase I bulk rock and petrological characteristics of the Phase I, II and III products from the literature.

Andesite Textures

Samples are generally crystal-rich (33-63 vol% phenocrysts), with a phenocryst assemblage dominated by plagioclase (64-78% of phenocrysts) complemented by lesser amphibole (8-28%), orthopyroxene (3-7%) and microphenocrysts of Fe-Ti oxides (1.5-3%). Maximum phenocryst sizes are typically ~7 mm for hornblende, ~3-4 mm for plagioclase and ~5 mm for orthopyroxene. Clinopyroxene microphenocrysts (< 1%) are present, as well as accessory apatite. Quartz is also present as rounded, embayed crystals sometimes jacketed by clinopyroxene. The variations in modal mineral contents are presented in Table 2.

The andesite groundmass is generally microcrystalline but can contain up to 25% rhyolitic glass in rapidly erupted samples. Cristobalite is present in slower erupted dense dome samples and can be up to 15 wt% in the groundmass, or more commonly as a vapor phase precipitate in the vesicles. The glass is commonly observed to have undergone phase separation and or devitrification in dome samples. Hornblende is replaced by orthopyroxene and clinopyroxene, thus yielding a groundmass normally comprising plagioclase, two pyroxenes and Fe-Ti oxides, with wide variations in microlite textures. No systematic differences in texture modal proportion or mineral composition have been observed within the andesites of Phases I, II and III (Table 2).

Enclave Textures

Mafic enclaves have been present in the eruptive products of the Soufrière Hills volcano as far back as 24ka (Wadge & Isaacs, 1988). The enclaves from Phases I, II and III are typically small (< 30cm) with a maximum reported length of 80 cm (Barclay et al., 2010; Plail et al., this volume); their shapes vary from ellipsoidal to angular. The ellipsoidal enclaves have smooth or crenulate, chilled contacts with the andesite. Small mm-scale fragments of enclaves are also observed in the andesite. The enclaves contain similar mineral phases to that of the andesite; they are however recognized by the higher abundance of mafic minerals, and a higher abundance of clinopyroxenes relative to orthopyroxene. There are no true phenocrysts present, but based on chemistry and texture there are andesite-derived xenocrysts of plagioclase, amphibole and orthopyroxene present in the enclaves.

The xenocryst contents can be up to 5% by volume for Phase I enclaves (Murphy et al., 1998; 2000), and up to 27% for Phase III; two thirds of which are normally plagioclase (Plail et al., this volume). The enclave groundmass is typically fine grained, consisting of randomly oriented interlocking elongate or acicular crystals of plagioclase, orthopyroxene, clinopyroxene and amphibole forming a diktytaxitic framework. About ~10% of residual rhyolitic glass with variable amounts of devitrification is observed in most thin sections, banded textures are also present in some scoriaceous samples.

Mineral Textures and Composition – (Andesite and Enclave)

Due to their similarities in crystal phases, the initial findings on the mineral compositions of the andesite and enclaves are both summarized together in this section. A through overview of the mineral chemistry from the early erupted products is presented in Barclay et al. (1998), Devine et al. (1998a; 1998b) and

Murphy et al. (1998; 2000) for Phase I and Humphreys et al. (2009a; 2009b) for the products of Phases II and III.

Plagioclase

Plagioclase is present as phenocrysts, microphenocrysts and microlites in the andesite with the phenocrysts showing a variety of zoning textures (Table 3; see also Murphy et al., 2000; Humphreys et al., 2009a; 2013). Oscillatory and patchy zoning are common in the phenocryst cores, including the cores of sieved crystals, which are interpreted to have experienced direct contact with melt of a more mafic nature. The modal proportion of each plagioclase textural type varies between samples. Plagioclase is present in the enclaves mostly as microlites, with minor inherited phenocryst from the andesite also present.

Plagioclase phenocrysts in the andesite have sodic cores (typically An_{48-58}, but with calcic zones up to An_{80}) with either normal or reversed zoned rims, while the microlites have more calcic cores An_{60-75} and can be normally, or to a lesser extent, reversed zoned. The plagioclase microlite cores in the enclaves are calcic up to An_{93} and normally zoned. Apart from the differences in anorthite content, the andesite phenocrysts generally have lower Fe contents than the enclave crystals. Most andesite microlites, some microphenocrysts and the sieved rims are generally richer in FeO content relative to the phenocryst rims, their elevated FeO contents are similar to that observed in the enclave plagioclase crystals (Figure 1e & f, Table 4).

Amphibole

Amphibole phenocrysts in the andesite show green-brown pleochroism and can show oscillatory zoning (Rutherford & Devine, 2003; Humphreys et al., 2009b). Amphiboles can have irregular rims (indicating slight resorption) or pristine rims, but commonly show a variety of breakdown textures, of which three

223 end-members can be identified (summarized from Devine et al., 1998a; Murphy et al., 2000; Rutherford
224 & Devine, 2003; Buckley et al., 2006; Humphreys et al., 2009b; Plechov et al., 2008):
225
226 (i) Fine-grained intergrowths of clinopyroxene, orthopyroxene, Fe-Ti oxides and plagioclase, growing
227 where the amphibole is in contact with melt. This breakdown texture can pseudomorph the original
228 crystal and is thought to form as a result of decompression during ascent due to changes in pH_2O.
229 The development of these rims can be used as an indicator of ascent conditions, with the thicker
230 rims developing during slower ascent. The rim thicknesses observed in the samples represent ascent
231 rates of > 0.019 m/s (Devine et al., 1998a; Rutherford & Devine, 2003).
232 (ii) Coarser-grained reaction rims dominated by clinopyroxene (preferentially aligned parallel to the c-
233 axis of the amphibole, and commonly in optical continuity). This rim type can also pseudomorph
234 the entire crystal and is interpreted as a thermal breakdown texture.
235 (iii) Partial to complete opacitisation, particularly along cleavage and cracks or adjacent to vesicles.
236
237 Decompression breakdown rims, thermal breakdown rims and resorbed rims are present in the majority of
238 analyzed samples; typically a given sample will also show a range of decompression rim thicknesses. In
239 the mafic enclaves, some amphibole microphenocrysts have undergone partial breakdown or opacitisation
240 while microlites are normally euhedral and yellowish in appearance. The inherited amphibole phenocrysts
241 in the enclaves most commonly show thermal breakdown textures. Amphibole compositions in the
242 andesite range from Mg-hornblende to Mg-hastingsite, with some pargasite present. Amphibole
243 compositions in the enclaves range from pargasite to Mg-hastingsite. In general, andesite amphibole
244 phenocrysts have lower Al_2O_3 (6-8 wt%) relative to the enclave amphibole contents of (12-14.5 wt%).
245
246 *Pyroxenes*
247 Orthopyroxene phenocrysts are typically euhedral, although some show slight rounding, which may be
248 followed by reversely zoned euhedral outer rims. The reversed zoned phenocrysts represent a minor

fraction of the total orthopyroxene population and are not observed in every thin section. Some crystals have rounded cores with clinopyroxene overgrowths. The reverse zoning is interpreted to occur as a result of heating, with the clinopyroxene overgrowth rims indicating direct contact with mafic melt. Clinopyroxene normally occurs in the andesite as microphenocrysts and microlites as well as overgrowths on orthopyroxene, quartz and sometimes in the thermal breakdown rims of amphibole (Table 3); it can be very common in the groundmass of some thin sections. Clinopyroxene is also common in mafic enclaves, as microlites and microphenocrysts.

There are three orthopyroxene phenocryst types, identified on the basis of having unzoned rims, reversely zoned rims or clinopyroxene overgrowths, all have similar core compositions (En_{56-70}, Fs_{26-41}, Mg# 63-68) where (Mg# = atomic units $Mg/(Mg+Fe^{2+})$). Type 1 consists of unzoned or weak normally zoned crystals with rim compositions En_{57-61} and $Wo_{1.8-2.3}$. Type 2 consists of reversed zoned crystals with rim compositions En_{62-73} and $Wo_{2.2-3.7}$.Type 3 consists of crystals with clinopyroxene overgrowths. Orthopyroxene microlites have Mg#s in the range 58-74 and display the second most magnesium rich compositions of the orthopyroxenes present in the andesite after the reversed zoned phenocryst rims (Table 6a & 6b). Orthopyroxene in the mafic enclaves have similar Mg#s to the andesite microlites. The clinopyroxenes have Mg#s in the range 66-74, and they are not in equilibrium with the orthopyroxene phenocrysts of the andesite.

Fe-Ti Oxides

In the andesite, phenocrysts are rare while microphenocrysts (>100 μm) are common and can be zoned (Table 3) with rounded irregular cores, resorbed rims and exsolved textures. Fe-Ti oxides also occur as inclusions in the phenocrysts and microphenocrysts of amphibole, pyroxene and plagioclase, where they tend to be subhedral. Enclave microphenocrysts can be euhedral homogeneous crystals or heterogeneous crystals with exsolution textures (Table 3).

Titanomagnetite is the most common oxide in the eruptive products, with minor ilmenite present. Individual hand specimen samples can show significant inter-crystal compositional variation; the extent of the variation can be such that Devine et al. (1998a) reported observing reversed zoning in half of the titanomagnetite crystals analyzed. The oxide compositions have shown little temporal variation for the first three eruption phases. The andesite titanomagnetite microlites and enclave titanomagnetites generally have higher titanium contents than the andesite microphenocrysts with the microphenocryst rims being slightly more titanium rich than the cores.

Bulk Rock Composition

To date only the Phase I bulk chemistry has been published, the products are predominantly andesite displaying SiO_2 contents in the range (58-62 wt%), (Murphy et al., 2000; Zellmer et al., 2003a; Barclay et al., 2010), with an average composition of 59.7 wt% SiO_2 (Murphy et al., 2000). The enclaves are reported to have SiO_2 contents of 51-56 wt% (Murphy et al., 2000) and 49-55.5 wt% (Zellmer et al., 2003a). Both compositions are low-K with the andesites having a calk-alkaline affinity while the enclaves are of tholeiitic affinity (Murphy et al., 2000). Bulk geochemical trends are similar in both lava types. With increasing SiO_2; TiO2, Al_2O_3, FeO, MgO and CaO all show decreasing trends, while Na_2O and K_2O show increasing trends. The Phase I andesites have relatively restricted major element compositions and the differences in the modal proportions of mineral phases were proposed as a likely source of the andesite heterogeneity within Phase I (Zellmer et al., 2003a).

Initial Conclusions

The experiments of Barclay et al. (1998) showed that the andesites were stored at a minimum pressure of 115-130 MPa at temperatures (820-840) ^{o}C before being erupted, with measured water contents in the range (4.27 ±0.54) wt% H_2O (Barclay et al., 1998), 4.7 wt% (Devine et al., 1998a) or up to 6.2 wt% H_2O (Humphreys et al., 2009b). Textural characteristics of the amphibole phenocrysts such as coarser grain

300 reaction rims dominated by clinopyroxene are thought to represent thermal breakdown during reheating
301 events, while partial to complete opacitisation, particularly along cleavage and cracks or adjacent to
302 vesicles is thought to develop during shallow dome storage with passive gas fluxing (e.g. Garcia &
303 Jacobson, 1979; Devine et al., 1998b; Humphreys et al., 2009b).
304
305 Couch et al. (2003b) proposed that the textural variations observed in the andesitic groundmass can be
306 attributed to variations in ascent rates in a system undergoing open system degassing. The presence of
307 enclaves in the erupted lavas (Murphy et al., 1998), the reverse zoning in the orthopyroxene and
308 plagioclase phenocrysts (Murphy et al., 1998; 2000) along with the higher temperature groundmass
309 assemblage (Humphreys et al., 2009a) were used as evidence that the eruption was triggered by an
310 intruding mafic magma, heating and remobilizing the andesite. It was also demonstrated that amphibole
311 fractionation is important in driving the enclave compositions (Zellmer et al., 2003a).
312
313 Reheated textures are fairly localized in the andesite (Murphy et al., 1998; 2000), which is evident in
314 the low modal abundance of reversed zoned plagioclase and orthopyroxene phenocrysts. Based on the
315 absence of amphibole microlites in the Phase I andesite, Murphy et al. (1998) had initially suggested that
316 enclave disaggregation was minor if at all present. More recently, Humphreys et al. (2009a) have shown
317 that the physical destruction and dispersion of some enclaves also contributes to the mafic nature of the
318 microlite assemblage in the Phase II and Phase III andesite groundmass, while Genareau & Clarke (2010)
319 showed that basaltic melt microscopically intrudes the margins of the andesite. Based on the thickness of
320 amphibole thermal breakdown rims, extrusion occurs after reheating on time scales of hours to months
321 (Devine et al., 2003; Rutherford & Devine, 2003; Devine & Rutherford, this volume).
322
323 Zellmer et al. (2003a) showed that the currently erupting Soufrière Hills andesite can be generated by
324 fractional crystallization of plagioclase and amphibole from the South Soufrière Hills (SSH) basalts. In
325 contrast, while the SSH lavas are compositionally similar to the mafic enclaves of the current Soufrière

Hills eruption (Figures 9 & 10), incompatible trace element ratios demonstrate that neither the current andesite nor the SSH lavas can be derived from the mafic enclaves (Zellmer et al., 2003a).

RESULTS

Phases IV and V

The textures of andesite samples erupted in Phases IV and V vary from the banded pumice produced during the July 28th 2008 explosion to the dome rock produced throughout both phases. We have already discussed how the volcanic activity of Phases IV and V differed to the first three extrusion phases; we now present the results of petrological and geochemical analysis from Phases IV and V.

Textures

The mineral phases present in the respective andesite and enclave lavas have remained consistent throughout the five eruption phases. Mineral textures associated with disequilibrium in Phases I, II and III andesites e.g. reversely zoned orthopyroxene phenocrysts, sieve textured plagioclase and embayed quartz are all observed in the andesites of Phases IV and V. Similarly to Phases I, II and III, amphibole is absent from the andesite microlite assemblage. Dome samples from Phases IV and V are generally crystal rich (~30-46% porphyritic) with phenocrysts and microphenocrysts of plagioclase, amphibole and orthopyroxene present along with microphenocrysts of clinopyroxene and Fe-Ti oxides (Figure 2). The groundmass in dome samples can be coarsely crystalline and vesicular (up to 35%) with microlites and glass present.

The enclave textures observed in Phases IV and V are also similar to those observed in the previous three phases. Plail et al. (this volume) categorizes the enclaves using parameters such as the volume of crystals inherited from the host andesite. They have identified three distinct enclave textures: a diktytaxitic framework dominated by plagioclase and pargasitic amphibole (Figure 3a); a diktytaxitic framework dominated by plagioclase and clinopyroxene (Figure 3b) and a composite (mixed enclave) of the above

two textures (Figure 3c). Xenocrysts (plagioclase, hornblende and orthopyroxene) are present in all enclave types (Plail et al., this volume).

The inter-phase differences between andesites of the eruption may be subtle. For example, some of the dome rock samples from Phases IV and V tend to be less dense and friable; their groundmass tends to be finer grained than the denser dome blocks. The feature seems more common in Phases IV and V relative to the earlier phases. Secondly, while the mafic enclaves are ubiquitous throughout the eruption, there is an apparent increase in enclave abundance over time (see discussion in Plail et al, this volume). The average macroscopic modal abundance of enclaves in the andesite products ranges from 1-2% in the Phase I products (Murphy et al., 1998; 2000) to up to 8% in the products of Phase III (Barclay et al., 2010) and 8.5 % in Phase V (Plail et al., this volume), while Komorowski et al. (2010) report a mafic content of 12% in the tephra generated from explosions during Phase IV activity (although these three sets of values were determined using different methods).

Banded Pumice

The banded sample from the July 28th 2008 explosion (sample number MVO1532d) is atypical of previously erupted samples. The sample shows clear textural heterogeneity in the form of whitish and dark grey streaks dissimilar to the chilled margins displayed by the mafic inclusions and resembles banded pumice. The sample comprises of a silicic part with pale brown to colourless glass, very few microlites and relatively low vesicularity, as well as a more mafic part which is dark brown with a crystalline groundmass and no obvious clear glass. Clearly mixed patches containing brownish glass are evident. The 'mixed' and mafic parts occur together spatially in patches hundreds of μm across, while the silicic parts form larger patches.

The mixed and mafic parts contain the typical assemblage present in the andesite such as phenocrysts of plagioclase with oscillatory and sieve textures, hornblendes, orthopyroxenes with clear rims or overgrown by clinopyroxene, and microlites of plagioclase + 2 pyroxenes + magnetite. In contrast, the silicic part

contains hornblende, no sieved plagioclase, only pristine orthopyroxene and few small microlites (~5-10 μm) of plagioclase, orthopyroxene and titanomagnetite; clinopyroxene is absent. Hornblende phenocrysts are commonly either pristine or have a very thin incipient reaction rims (5-8 μm). The silicic matrix also contains numerous larger (50-200 μm) broken fragments of plagioclase phenocrysts. Euhedral, prismatic quartz microlites are common; these are normally ~50 μm (±20) in size and are not typical of the Soufrière Hills andesite. They do not replace the typical rounded, embayed quartz phenocrysts, which are present as usual.

Plagioclase Composition

The Phase IV and Phase V andesite plagioclase phenocryst cores and rims exhibit a wide range of compositions (An_{46} to $>An_{80}$, Table 4) which overlaps with phenocryst compositions from the previous phases (Figure 1a). The oscillatory plagioclase cores are generally more calcic than the cores of phenocrysts with other textures (Figure 1d). The mean An content for both Phase IV and Phase V phenocryst rims is ~ An_{56}, within error of the mean An contents from phenocryst rims of the previous phases (Table 4, Figure 1a). As with the first three extrusion phases, the microlite rims of Phases IV and V are more calcic than their respective phenocryst rims (Figure 1a & b, Table 4), and the enclave microlites are generally more calcic than the andesite microlites (Figure 1b). There is inter-phase variation of Fe contents in the andesite hosted microlite crystals, it is however non-systematic.

Amphibole Composition

Phase IV and Phase V andesite amphiboles are predominantly magnesio-hornblende, the same as the andesite amphiboles from Phases I to III (Figure 4a) with minor amounts of tschermakite. Mg-numbers are in the range 0.44-0.55. There is a systematic change in enclave amphibole FeO content (Figure 4d) from Phases I to III (unfortunately, no data from Phase IV enclave amphibole is available since no enclave products from Phase IV were collected). The enclave amphiboles from Phases I to III display a

steady increase in magnesium numbers (0.5 to 0.59), and the SiO_2 content also decreases from Phases I to III (Table 5b, Figure 4c &d). The absence of Phase IV enclave amphibole data produces an undesired gap in the dataset however, it can be seen that the Phase V enclave amphibole have higher mean contents of wt% Al_2O_3, MgO, CaO, TiO_2 and Na_2O relative to the amphibole in the enclaves of the first three eruption phases (Table 5b). Apart from having the highest FeO and SiO_2 contents, the Phase I enclave amphiboles are lowest in wt% Al_2O_3, MgO and TiO_2.

Orthopyroxene Composition

Andesite orthopyroxene phenocryst core compositions have been relatively homogeneous throughout the eruption (En_{56-70}, Fs_{26-41}) with a mean magnesium number of 0.6 (Table 6a). The normally zoned rims (Mg# 0.58-0.65 mean ~ 0.61) and reversed zoned rims (Mg# 0.68-0.75 mean ~ 0.7) have been fairly unchanged during the eruption (Figure 5a). The andesite microlites generally have higher magnesium numbers, as well as higher CaO and Al_2O_3 contents, than the phenocryst cores throughout the eruption (Figure 5b). Microlites from Phases I, II, III and IV have the same mean magnesium number of 0.67 (Figure 5b). However, the microlites of Phase V have a slightly lower mean magnesium number of 0.63 (Table 6a, Figure 5b).

Clinopyroxene Composition

The clinopyroxene composition has varied little throughout the eruption; they are mostly augites, calcic-augites and diopsides with cores and rims in the compositional range En_{39-49}, Wo_{31-47} and mean compositions of En_{42-44}, Wo_{40-43}. Kushiro (1960) has demonstrated that it is the SiO_2 wt% content of a magma and not temperature that is the major control of the SiO_2/Al_2O_3 ratio of the crystallizing clinopyroxenes and that the ratio increases with increasing magma SiO_2 content. The andesite clinopyroxenes show distinct SiO_2/Al_2O_3 ratios by eruption phase (Table 6c). The enclave clinopyroxenes also show a similar inter-phase trend in FeO from Phase I to III like the enclave amphiboles.

Oxide Composition

As was the case in the first three eruptive phases, titanomagnetite is the most common oxide in the products of Phases IV and V with only minor ilmenite present. The andesite microphenocryst titanomagnetite cores and rims from the five extrusion phases have overlapping compositions (21-30 mol% Usp), with no systematic variation between phases. The Phase IV microlites have higher TiO_2 contents (up to 16 wt%) than the microphenocrysts (7-10 wt%), as is the case with the titanomagnetites from Phases I, II and III. However, this is not the case for Phase V where the microlites have similar TiO_2 wt% contents to the microphenocrysts from Phase V (Table 7a).

Glass composition

The andesite and enclave glass compositions for the products of Phases IV and V have shown little variation relative to the previous phases, glass compositions have been consistently rhyolitic in both magma types (70-82 wt% SiO_2) throughout the eruption (Table 8). Some authors have shown that the glass present in both magma types are essentially indistinguishable (e.g. Murphy et al., 1998; 2000), while others (e.g. Humphreys et al., 2010) have shown evidence indicating subtle differences between enclave and andesite glass. The K_2O content shows a bimodal distribution of high and low K_2O glass samples with some intermediate compositions observed (Figure 6).

Humphreys et al. (2010) interpreted the glass compositions enriched only in K_2O, as an indication of diffusive contamination by high-K mafic inclusion glass; some samples are also enriched in TiO_2, suggesting physical mixing of remnant glass. In general with increasing SiO_2, there is a decreasing trend of Al_2O_3, while K_2O increases (Figure 6). There are a few samples with SiO_2 contents of 80-82 wt% that have high Na_2O, high CaO, low FeO and low K_2O, which are likely due to post extrusion phase

452 separation of two types of glasses of differing chemistry as described by Cashman (1992) for the Mt St
453 Helens lava dome and indicated by Humphreys et al. (2009a) for the products of Phases II and III.
454
455 *Bulk Rock Composition*
456 The andesites of Phases IV and V have a similar range in bulk rock SiO_2 (56-62 wt%) to the products of
457 the previous phases (Table 9). The trends of decreasing TiO_2, Al_2O_3, FeO, MgO and CaO and increasing
458 Na_2O and K_2O with evolution reported for the Phase I products are present in the products of the later
459 eruptive phases (Figure 7). There is considerable inter-phase compositional overlap for most elements at
460 similar SiO_2 contents. As is the case with the andesite, the enclave products of the later phases show
461 compositional overlap and similar trends to the Phase I enclave products.
462
463 *Whole Eruption*
464 *Trends and Variations in Bulk Rock Composition*
465 There are some clear differences between the eruption phases in terms of bulk rock composition. Firstly,
466 the FeO contents show systematic inter-phase variation with the mean FeO contents showing a clear
467 decrease during the first three phases. The andesite products of Phase I have a mean FeO content of (7.32
468 wt%), while the Phase II and Phase III products have mean values of 7.14 and 6.6 wt% FeO respectively
469 (Table 9). There is a relative increase in mean FeO to 7.4 wt%, for samples erupted during Phase IV
470 followed by a subsequent decrease in Phase V to 7.08 wt% FeO (Figure 8a, Table 9). Although not as
471 systematic as FeO, MgO contents also show some variation in the andesite (Table 9).
472
473 The enclave bulk rock FeO trend behaves in a similar way to the andesite bulk FeO trend (Figure 8a).
474 The inter-phase contrast in FeO content is however more pronounced in the enclaves than in the
475 andesites, thus at approximately 50 wt% SiO_2 there is a bulk rock compositional difference of up to 2
476 wt% FeO between the enclave products of Phases I and III (Figure 7). One observation of note is that the
477 difference between the mean bulk enclave FeO content and their syn-eruptive host andesites shows a

steady decrease with a change of ~ 1% over the eruption, from 2.3 wt% in Phase I to1.4 wt% in Phase V, this is outside the error of the FeO contents. In other words, the difference between enclave and host FeO contents has been narrowing with time. There are also subtle differences in MgO and CaO that are outside analytical error.

Also of note is that the Phase I and Phase II andesite compositions are more scattered than those of Phases III, IV and V (Figures 7 & 10). This results in better defined linear trends of (for example) Al_2O_3, CaO, TiO_2 and Sc with increasing FeO/MgO for the andesite products from Phases III, IV and V; linear trends are also present in the enclave products of Phases III and V (Figure 10). There is a bit of scatter at higher ratios (>2.2 FeO/MgO) in the Phase III and Phase V enclaves in all of the plots. The enclave products of Phases III and V define a different slope to the Phase I and Phase II products on the SiO_2 vs. FeO plot (Figure 7) and thus together seem distinct from the products of Phases I and II. Phase IV enclave data are not available, but given the behaviour of the Phase IV andesite products and the apparently coupled FeO variation of both magmas, we anticipate that the bulk chemistry of the Phase IV enclaves would quite likely show well defined trends with little scatter similar to that observed in the enclaves of Phases III and V. It must be noted that the inter-phase variation in plagioclase microlite FeO content (Figure 8d) does not mirror bulk rock inter-phase FeO variation (Figure 8a).

Generally, the Phase V andesites have the highest SiO_2 contents while the Phase II and Phase IV andesites have the lowest SiO_2 contents. The Phase V enclaves are also the most SiO_2-rich (Plail et al., this volume); regardless to this the SiO_2 contents of the enclaves and host andesites are not coupled. This is highlighted by the Phase II enclaves being more SiO_2-rich than the Phase I and Phase III enclaves (Table 9). The Phase V andesites also show elevated total alkali contents, relative to Phases I, III and IV andesites (Figure 5c) as well as lower wt% TiO_2, Al_2O_3, MgO and CaO (Table 9). Phase IV andesites have the highest wt% FeO, MgO and Al_2O_3 while the Phase II andesites are richer in CaO wt%. The Phase V enclaves are richer in total alkalis.

504

505 Due to its amalgamated nature, the integrity of the bulk rock data set needs be examined in order to verify
506 whether the observed variations in FeO are real or an artifact of using different laboratories over several
507 years. This is addressed in Appendix I where we show that the observed variations are independent of
508 laboratory bias and are indeed real.

509

510 *Estimates of temperature, pressure, water content and log fO2*

511 A number of different methods have been used to estimate the pre eruption temperatures of the andesites
512 and mafic enclaves, including estimates obtained from orthopyroxene (using QUILF, Anderson et al.,
513 1993) in single pyroxene mode, following Murphy et al. (2000), use of magnetite-ilmenite pairs (e.g.
514 Devine et al., 2003), the hornblende-plagioclase geothermometer of (Blundy & Holland, 1990), the 2-
515 pyroxene geothermometer of Lindsley (1983), the plagioclase-liquid thermometer of (Putirka, 2005), and
516 clinopyroxene-melt equilibria of Armienti et al. (2007), after Putirka et al. (1996; 2003) and Putirka
517 (1999) which also produces pressure estimates. Pressures were also estimated with VolatileCalc
518 (Newman & Lowenstern, 2002) by measuring glass volatile contents and assuming H_2O saturation.

519

520 For Phase I, these approaches generated values of 785-980 ^{o}C for the andesite orthopyroxene phenocryst
521 cores with an average of 851 ±20 ^{o}C (Murphy et al., 1998; 2000), a similar temperature range of 834-850
522 ^{o}C was obtained by Devine et al. (1998a), and 820-840 ^{o}C by Devine et al. (2003) both using magnetite-
523 ilmenite phenocryst pairs. This is consistent with the experiments of Barclay et al. (1998) which showed
524 that the andesites were stored at temperatures 820-840 ^{o}C before being erupted. The reversed zoned
525 orthopyroxene rims give higher temperatures up to1100 ^{o}C (Murphy et al., 1998; 2000). Enclave hosted
526 orthopyroxene cores give temperatures in the range 1020-1050 ^{o}C (Murphy et al., 1998). New data
527 obtained by MVO for Phases II,III,IV and V (some Phase II and Phase III data reported in Humphreys et
528 al., 2009a) are reported below and presented in Table 11.

529

Pyroxene: Orthopyroxene phenocryst cores in the andesite give temperatures of 824-965 °C (mean 866 °C), with unzoned rims at 845-895 °C (mean 869 °C) and reversely zoned rims at 1018-1032 °C (mean 1025 °C). Orthopyroxene inclusions in other minerals or in crystal clots also gave low temperatures791-809 °C. Orthopyroxene microlites in the andesite gave temperatures of 958-1017 °C, while orthopyroxene in mafic enclaves gave 903-1305 °C (mean 1070 °C), with 1074-1196 °C for the two-pyroxene geothermometer. These two-pyroxene temperatures may not reflect equilibrium conditions.

Plagioclase-liquid: the plagioclase-liquid thermometer produced a wide range of temperatures from 821 °C (for melt inclusions trapped in plagioclase phenocrysts) to 1100 °C (for matrix glasses paired with microlite rims); with increasing temperatures correlating with decreasing melt H_2O content. This is similar to the style of variation reported in Blundy et al. (2006) but given the huge range in temperature we suggest that many of the higher groundmass temperatures may reflect disequilibrium.

Hornblende-plagioclase: Inclusions of plagioclase in andesite hornblende phenocrysts give temperatures in the range 804-890 °C (mean 833 °C). Paired analyses from crystal clusters, interpreted as fragments of disaggregated mafic enclaves, give temperatures of 849-947 °C (mean 894 °C).

Clinopyroxene-melt: The clinopyroxene-melt thermometer gave temperatures in the range 1097-1145 °C (mean 1110 °C) for microlites/matrix glass and microphenocrysts/matrix glass in the mafic enclaves. As with the two-pyroxene and plagioclase-melt temperatures, these may not reflect equilibrium conditions.

Pressure and water estimates: Pressure estimates obtained from the Cpx-melt equilibrium for crystals from both enclaves and andesite range from 10-280 MPa with a mode of 50-100 MPa. Previous measurements of melt H_2O contents from melt inclusions are in the range 4.27 ± 0.54 wt% H_2O (Barclay et al., 1998), ~4.7 wt% (Devine et al., 1998a) and 1.1-6.2 wt% (Humphreys et al., 2009b). Assuming water saturation in the absence of CO_2 (Newman & Lowenstern, 2002), these estimates equate to pressures up to 214 MPa which is consistent with the estimates from the Cpx-melt equilibrium.

Temperature variation

Different methods tend to produce distinct temperature ranges and this is probably because they are recording temperatures from different parts of the reservoir or localized equilibrium at differing times. Taken together, the hb-plag temperatures, single-orthopyroxene core temperatures, 2-oxide temperatures and plagioclase-liquid temperatures from melt inclusions are probably representative of phenocryst crystallization and hence the ambient temperature within the andesite storage region. These temperatures are typically in the range 785-900 °C with an average at the lower end of that range and are consistent with the experiments of Barclay et al. (1998) on Phase I products.

Higher temperature estimates are obtained from the disequilibrium features outlined above, e.g. 826-1101 ° C from reverse zoned orthopyroxene rims (Table 11). This is consistent with the very An-rich compositions observed in sieved plagioclase crystals, which requires very high temperatures and a more mafic melt (Couch et al., 2003a). These temperatures are inferred to be recording the reheating of the andesite crystals by the basalt intruding into the base of the reservoir. The estimates from the enclaves are expectedly higher, 903-1305 ^{o}C for the single orthopyroxene method, 1074-1196 ^{o}C using the 2 pyroxene method and 1097-1145 ^{o}C using the clinopyroxene-melt equilibrium, although some of these temperatures may also reflect disequilibrium mineral compositions.

The variability within these estimates may be due to heterogeneities within the andesite storage region, and/or due to the localized nature of the basaltic intrusion and thus equilibrium at higher temperatures (e.g. Pichavant et al., 2007). The temperature estimates obtained using the various methods all show a range of values with the smallest difference between maximum and minimum temperatures being 14^{o}C for any given method. There is no evidence in our data to suggest systematic changes in temperature as the eruption proceeds. However Devine & Rutherford (this volume) used oxide thermometry to show that the mean ambient temperature of the andesite before being reheated shows a 10 ^{o}C increase from Phase I (825 ^{o}C) to Phase V (835 ^{o}C).

582 *Estimates of log fO2*

583 Log *f*O2 values calculated from andesite hosted ilmenite-magnetite pairs are presented in Table 8. The
584 inter-phase values show some overlap with no clear trend. The Mg-Fe exchange coefficient Kd, (Putirka
585 et al., 2003) is used to establish mineral melt equilibrium of clinopryroxenes where Kd cpx-liq = [(*X* MgO
586 liq/ *X* FeO Cpx) / (*X* MgO Cpx/ *X* FeO liq)]. Suitable mineral-melt equilibrium is thought to be attained
587 when a Kd value of 0.27±0.03 is obtained for clinopyroxene. Bèdard (2010) showed that clinopyroxene
588 Kd values will vary as a function of temperature, pressure, log fO_2 as well as melt SiO_2 and, total alkalis.
589 Box plots of clinopyroxene microlite Kd values by eruption phase are presented in Figure 5d, the Kd
590 value for the clinopyroxene microlites varies by eruption phase with Phase III having the highest median
591 values while Phases V and II have the lowest median values. The data obtained from the Cpx-melt
592 equilibria showed no systematic variation in pressure and temperature with eruption phase. The total
593 alkali contents display a negative correlation with the clinopyroxene Kd values, hence it seems the Cpx
594 Kd values are responding to changes in total alkali content and not log fO_2.
595

596 **DISCUSSION**

597 Although the andesitic rocks erupted since 1995 at Soufrière Hills are fundamentally similar in terms of
598 textures and mineral compositions, there are some key systematic variations over time that may reveal
599 details about the nature of the plumbing system at depth. In particular, the key observation is that the bulk
600 rock FeO content of both andesite and enclave appear to be coupled. Both andesites and enclaves from
601 Phases I and II show higher major element oxide contents apart from SiO_2, and more scatter at similar
602 FeO/MgO ratios compared with the later phases (Figure 10), they also have higher CaO/Al_2O_3 ratios at
603 similar FeO/MgO ratios. Here we review the overall relationships between the andesite and enclave
604 magmas and hence interpret the possible causes of these compositional variations.
605

606 Mt Pelée Martinique has produced a spectrum of products ranging from basaltic-andesites to dacites;
607 some compositions were only erupted at certain periods in the volcano's history due to the changing
608 nature of volcano's plumbing system with time (Fichaut et al., 1989a). Andesites are however ubiquitous
609 in the Mt Pelée deposits and have been of a similar composition for the past 100,000 years (Dupuy et al.,
610 1985). The Mt Pelée andesites also contain microlites inherited from intruding basalts (Martel et al.,
611 2006) as do the Soufrière Hills andesites (Humphreys et al., 2009a).

612 The volcanic stratigraphy and petrology of Mt Pelée, is well constrained and the physical evolution of the
613 plumbing system through time has been modeled (Fichaut et al., 1989a). It has been established that the
614 current shallow reservoir is zoned (Dupuy et al., 1985, Pichavant et al., 2002) and is relatively small (<
615 $1km^3$) at about 10km bsl (Fichaut et al., 1989a). It has also been established that the basaltic magmas are
616 parental to the andesites via magma mixing and fractional crystallization (Fichaut et al., 1989b).

617

618 Magma mixing occurs in relation to basaltic intrusions which generate eruptions with heterogeneous
619 magma compositions (e.g. Fichaut et al., 1989a; Gourgaud et al., 1989), they are normally larger in
620 volume than the homogeneous eruptions since lower parts of the reservoir gets tapped (Dupuy et al.,
621 1985). Fractional crystallization of the hybrid magmas created by the mixing events produces fairly
622 homogeneous magmas which tend to evolve towards more acid compositions; these are the magmas that
623 feed the smaller volume homogeneous eruptions (Fichaut et al., 1989a; Pichavant et al., 2002). Thus
624 andesite generation at Mt Pelée is fairly well understood.

625

626 *Andesite phenocryst-groundmass relationship*

627 In the current Soufrière Hills eruption, microlite rims and some cores are generally more mafic than
628 phenocryst rims (in the case of plagioclase) or both cores and rims (in the case of orthopyroxene). This is
629 contrary to what is expected from closed-system crystallization and cooling, and demonstrates the effects

of mafic magma input and the short time scale between heating and eruption. The nature and extent of physical interaction between the andesites and basalts is also evidenced in the ubiquitous presence of mafic enclaves within the andesite, as well as rarer macroscopic features such as the banded pumice. The contrasting temperatures of the intruding mafic magma and the silicic host also leads to heat transfer (Snyder, 2000), resulting in remobilization of the andesite (Murphy et al., 2000).

The andesite contains various disequilibrium textures which provide evidence of reheating driven by mafic magma, including reverse zoned orthopyroxene (Barclay et al., 1998; Murphy et al., 1998; 2000); sieve textures and calcic overgrowth rims on plagioclase phenocrysts (Couch et al., 2003a); two oxide disequilibrium (Devine et al., 1998a; 2003); resorbed quartz with clinopyroxene mantles; thermal breakdown of amphiboles (Humphreys et al., 2009b); and clinopyroxene overgrowths on orthopyroxene (Murphy et al., 1998; Humphreys et al., 2009a). These observations are consistent with the higher range of temperatures obtained from the andesite by some of the thermometry methods employed.

Other Disequilibrium Features

The andesite microlite assemblage generally consists of normally zoned plagioclase with euhedral to hopper or skeletal textures (suggesting rapid growth, Hammer & Rutherford, 2002), normally zoned orthopyroxenes, and normally zoned clinopyroxenes with a skeletal appearance. Although all orthopyroxene microlites are typically more mafic than phenocryst rims, they are not always compositionally identical to the enclave microlites, but can sometimes exhibit intermediate or even more mafic compositions relative to some enclave microlites (Figure 5b).

The absence of groundmass amphibole in the Phase I andesite and the proposed compositional differences between the plagioclase groundmass in the Phase I andesite and the enclave plagioclase were used as evidence against enclave disaggregation being a significant process (Murphy et al., 2000), the absence of groundmass amphibole in the andesite was also used by Couch et al. (2003a) as evidence against magma

656 mixing. More recently (Humphreys et al., 2009a; Genareau & Clarke, 2010; Humphreys et al., 2010)
657 proposed enclave disaggregation and mixing as significant processes to support chemical and textural
658 observations in the products of Phases II, III and IV.
659
660 We have also shown that the Phase I andesite plagioclase microlite population has elevated Fe contents
661 similar to the enclave plagioclase and the andesite microlites from subsequent phases (Table 4, Figure
662 1e), which suggests that disaggregation probably did occur during Phase I. We have also highlighted the
663 dominance of normally zoned plagioclase microlites in the andesite. These additional observations
664 suggest that the mafic signature of the Soufrière Hills andesite groundmass may not be due to a simple
665 case of crystal transfer due to enclave disaggregation, and that reheating and recrystallization of resident
666 crystals might also be an important process in generating the hotter groundmass assemblage. The lack of
667 change in modal abundance of reverse zoned plagioclase and orthopyroxene phenocryst indicates that the
668 heating is still ongoing on a scale that has remained relatively unchanged. Finally, we suggest that the
669 dominance of normally zoned plagioclase microlites reflects decompression-driven crystallization
670 continuing after enclave disaggregation.
671
672 The microprobe SiO_2/Al_2O_3 ratio of crystallizing clinopyroxene is heavily dependent on the bulk wt%
673 SiO_2 content of the host magma (Kushiro, 1960); with increasing bulk rock SiO_2 favouring increased
674 SiO_2/Al_2O_3 ratios in the cpx crystals. Thus the higher SiO_2/Al_2O_3 values of the Phase V microphenocrysts
675 (Table 6c) suggests that the clinopyroxene microphenocrysts found in Phase V andesites crystallized in a
676 more SiO_2-rich melt relative to the microphenocrysts from the first three phases. There are a number of
677 other observations for the Phase V andesites such as the elevated total bulk rock alkali contents relative to
678 Phases I, III and IV andesites (Figure 5c); lower TiO_2 wt% contents in the oxide microlites (Table 7a) and
679 the slightly lower magnesium numbers of the orthopyroxene microlites (0.63) (Table 6a, Figure 5b) that
680 are all consistent with the Phase V andesite products being more evolved.
681

682 *Bulk Rock Variation*

683 *Enclave Compositions*

684 The fundamental trends in the enclaves are related to fractional crystallization. The enclave products of
685 Phases I and II are much more scattered compositionally (Figure 10). We interpret the scatter in the Phase
686 I and Phase II enclaves as an indication of assimilation of plutonic residues remaining from previous
687 mafic injections. There is a bit of scatter in the more evolved samples (>2.2 FeO/MgO) of the Phase III
688 and Phase V enclaves in all of the plots; the linear trends observed in the enclave products of Phases III
689 and V could be consistent with fractional crystallization, less affected by assimilation processes. Hence
690 the minimal scatter in the Phase III and Phase V enclaves indicates they may have erupted through a
691 relatively residue-free pathway.

692

693 Irrespective of the scatter present in the products of Phases I and II there are still discrepancies in
694 compositions of the enclave products that need to be accounted for. The ratios of incompatible trace
695 elements should not be affected by shallow crustal process therefore; incompatible trace element ratios
696 should be representative of the source region. The near constant ratio of Zr/Rb in the mafic enclaves
697 (Table 10) indicates a fairly homogeneous source composition and suggests that the observed major
698 element differences are likely due to differentiation rather than heterogeneities in the source region. There
699 are a number of possible processes that might cause the enclave compositions to change and to better
700 constrain why, we address the following relevant questions.

701

702 i. Are the discrepancies purely due to the effects of contamination, thus are Phase I and Phase II
703 enclaves more hybridized products of the same magma, parental to the products of Phases III and
704 V?
705 ii. Are the enclave compositions representing localized compositions in a chemically heterogeneous
706 basaltic system?

iii. Do the enclaves of each phase represent discrete chemically distinct batches of basalt magma from depth?

Assimilation of plutonic residue

Earthquake swarms in the century leading up to the current eruption were considered to represent the intrusion of basalt into the andesite storage area (Shepherd et al., 1971). The mafic magma interacting with the andesite will over time cool and crystallize, resulting in crystals accumulating at the base of the reservoir. Subsequent intrusions of basalt may therefore interact with any crystal mush or plutonic residue present, assimilating crystals and creating hybridized liquid compositions. Thus it is possible that the primary magma composition intruding into the andesite reservoir has not changed with time, but the compositions of the early erupted products of Phases I and II are driven by contamination from residue left from previous basaltic intrusions into the andesite reservoir. If this were the case, then the bulk chemistry for enclave products from Phases III and V should be generally more basic than the products of Phases I and II, and the bulk enclave compositions of the Phases I and II should be reproducible by addition of crystals to the bulk enclave compositions of Phases III and V.

There are a number of observations inconsistent with this model. First is that most recent enclave products of Phase V are more evolved than the earlier enclave products (Plail et al this volume). Secondly, crystal accumulation would increase the SiO_2 contents of the Phase I and Phase II enclave products and drive them towards the compositions of the Phase III and Phase V enclave products on the SiO_2 vs. FeO/MgO plot (Figure 10). Thus there is therefore no evidence to suggest that the enclave compositions of Phases III and V represent less hybridized liquids of the same magma batch that produced the enclaves of Phases I and II and we therefore reject this theory. This however indicates that there are other processes influencing the enclave compositions other than simple crystal assimilation and fractional crystallization.

733 *Stratified reservoir*

734 Chemical heterogeneity within a magma reservoir could be characterized by vertical compositional
735 stratification due to the relationships between magma density and chemistry, with the less evolved, denser
736 magmas residing in the lower regions of the reservoir (e.g. Trail and Spera, 1990), as is the case in the
737 present day reservoir of Mt Pelée (e.g. Dupuy et al., 1985, Pichavant et al., 2002). Continuous or periodic
738 tapping of a vertically heterogeneous reservoir is thus expected to produce a compositional variation
739 towards lesser evolved lavas as the deeper reservoir is tapped, but this is inconsistent with the more
740 evolved nature of the Phase V enclaves (Plail et al this volume); therefore we do not accept this model for
741 explaining the inter-phase enclave and andesite compositional variations.

742

743 *Distinct chemical pulses*

744 The nickel contents of the enclaves are all <20 ppm and they are hence not representative of primary
745 compositions, which would be expected to have 200-300 ppm nickel (Rhodes & Dungan, 1977). The
746 absence of modal olivine and the presence of modal plagioclase are also consistent with the parental
747 compositions of the enclaves not being primary. Therefore the magma injected into the base of the
748 andesite reservoir must have previously undergone differentiation, most recently in the deeper reservoir of
749 the Soufrière Hills magma system at 10-13km (e.g. Elsworth et al., 2008; Foroozan et al., 2010; 2011).
750 This is consistent with the fractional crystallization trends present in the Phase III and Phase V enclaves.
751 However, the nature of basalt delivery into the base of the Soufrière Hills andesite reservoir is still a
752 matter of discussion. A scenario of continuous recharge is proposed by Wadge et al. (2010) and Foroozan
753 et al. (2011) due to the patterns observed in the GPS deformation signal. Contrary to this, Humphreys et
754 al. (2009b) showed that the amphibole phenocrysts in the andesites have variations in their molar (Cl/OH)
755 ratios and temperatures attributed to non-continuous volatile release which likely coincide with basalt
756 recharge episodes.

757

If the basalt input into the base of the andesite reservoir is pulsed, then the enclaves from each eruption phase may represent chemically distinct magma pulses entering the andesite reservoir. The liquids likely represent melts from the same reservoir whose compositions are being driven by differentiation processes occurring on timescales shorter than that of the eruption. Edwards & Russell (1998) have demonstrated that AFC processes in basalts can occur on the time scale of weeks to years, a timescale which is consistent with the timescale of the first three extrusion phases and intermediate pauses. This model of periodic basalt delivery is also consistent with the observations of periodic heating Zellmer et al. (2003b), periodic volatile release Humphreys et al. (2009b) and the short time scales of hours to months between reheating, mixing and eruption of the hybrid material (e.g. Snyder, 2000; Devine et al., 2003; Humphreys et al., 2010; Devine & Rutherford, this volume). This model is thus consistent with the petrological and geochemical data and is therefore accepted as a possible cause for the basalt compositional variation.

Enclave Amphibole

We have demonstrated that the inter-phase variation of FeO content in enclave amphibole mirrors FeO variation in the bulk rock for the first three extrusion phases (Figure 4d, Figure 8a), and that there is a systematic inter-phase increase in the enclave amphibole Mg# (Figure 4c, Table 5b), and an inter-phase trend of increasing Mg and Al with falling Si from Phases I to III (Table 5b).

The composition of amphibole is heavily influenced by the composition of the liquid from which they crystallize. In particular, the Al content is related to crystallization pressure (Hammarstrom & Zen, 1986; Hollister et al., 1987; Johnson & Rutherford, 1989; Rutter et al., 1989; Blundy & Holland, 1990; Schmidt, 1992; Devine et al., 1998a; Ernst & Liu, 1998; Ridolfi et al., 2010). This is consistent with the experimental data of Barclay et al. (1998) which showed that higher pressure crystallization runs on the Soufrière Hills andesite products produced amphiboles with higher Al contents than the amphiboles which occurred naturally in the lavas. Variations in amphibole Al content can also be influenced by temperature and fO_2 (Bachmann & Dungan, 2002; Anderson & Smith, 1995). In general for calcic

784 amphiboles, increasing P and T leads to increases in MgO, Mg# and Al, while decreases in Si along with
785 total (Fe + Mn + Ca) can also expected.
786
787 There are no independent crystallization temperature estimates for the enclave amphiboles and hence no
788 way to assess how much influence the temperature or pressure has on the enclave amphibole Al contents.
789 The increasing Mg#s in the enclave amphiboles from Phases I to III are consistent with the parental
790 magmas becoming increasingly mafic from Phase I to Phase III. This would also explain the decreasing
791 Si and increasing Al, and would be consistent with increasing crystallization temperatures. We do note
792 however that the high Al and Ca contents coupled with high Mg#s of the Phase V enclave amphiboles
793 (Table 5b) is inconsistent with the more evolved nature of the host magmas as indicated by Plail et al.
794 (this volume). We also note that the lack of systematic inter-phase variation in the andesite-derived
795 amphiboles is consistent with fairly stable crystallization conditions.
796
797 To summarize, the pattern of varying bulk rock enclave compositions is consistent with temporal
798 variations in the composition of the parental mafic magma entering the volcanic system at depth. This can
799 also explain the coupled changes in enclave amphibole composition, which is consistent with
800 crystallization from an increasingly more mafic melt for the first three extrusion phases.
801
802 *Andesite Compositions*
803 The observed chemical heterogeneities in the Phase I andesitic products are attributed by Murphy et al.
804 (2000) to the proposed mode of formation, which is mainly the disaggregation and remobilization of
805 multiple previously intruded andesitic bodies. The scatter present in the Phase I andesite is similar to that
806 observed in the Phase I enclaves; and lessening of the scatter as the eruption proceeds is also present in
807 the andesite as well as the enclaves. The behaviour of FeO in both lava types suggests that the
808 composition of both is coupled to some extent, but the reason for this is not clear. We suggest that the
809 bulk andesite compositions may be dependent on the composition of the syn-erupted basalt with which it

interacts, inheriting the geochemical imprint of the mafic magma. Below we consider the possible mechanisms for transferring such a geochemical signature from the mafic magma to the andesite.

Andesite Hybridization

Hybridization requires mass transfer which has been shown to occur at the Soufrière Hills with the proposed processes ranging from simple crystal transfer, (Murphy et al., 1998; 2000) to the physical destruction of the enclaves by varying mechanisms (e.g. Humphreys et al., 2009a; Edmonds et al., this volume; Plail et al, this volume), to localized mixing, percolation and incorporation of melt into the host andesite margins (Genareau & Clarke, 2010). It must be noted that although not systematic and coupled like FeO, inter-phase variation is still observed in all of the major elements of both lava types. The elevated Ca, Al and Mg contents of the groundmass assemblage makes it apparent that Fe is being systematically transferred from the enclaves to the host andesite while the other major elements are transferred on a more irregular basis. Therefore the process/processes responsible for transferring the Fe signature from enclave to andesite must be examined.

Enclave disaggregation

Variations in the FeO contents of enclave clinopyroxene and amphibole are similar to the observed bulk rock variations, while no systematic variation in FeO is observed for any of the other enclave mineral phases. We therefore suggest that a possible explanation for the bulk rock compositional variation is the physical destruction of mafic enclaves, and incorporation of clinopyroxene and amphibole crystal fragments into the andesite. The presence of high-Al amphibole fragments in the groundmass of Phase II and Phase III andesite supports such a process.

This model was tested by performing mass balance calculations on the andesite compositions using FeO content as the index for choosing end members, which are the low FeO and high FeO samples within each eruption phase. We use the enclave mineral compositions present in each respective phase for the

836 calculations. If enclave destruction is responsible for the Fe signature in the andesite then the mass
837 balance results should be consistent with the low modal occurrence of high Al amphibole fragments in the
838 groundmass. However, the goodness of fit (reflected by R^2 values) for our modeled results is rather low,
839 and the results show that the required mass of crystals to be added is inconsistent with the observed
840 modes (Table 12). Therefore this model for Fe transfer is rejected.
841
842 *Diffusion/advection from enclaves*
843 Grasset & Albarede (1994), propose a mechanism whereby diffusion and buoyancy-driven convection are
844 responsible for the chemical exchange between mafic enclaves and their hosts. They propose that the
845 density difference between the enclave and host will induce relative motion which entrains the enclave-
846 host interface thus generating a flow pattern inside the enclave. Thermal equilibrium occurs on much
847 shorter time scales than chemical equilibrium via diffusion (Sparks & Marshall, 1996) thus hybridization
848 by chemical diffusion requires both magmas be liquid and the presence of mobile fluids for transporting
849 the chemical species.
850
851 The chilled margins and abundant interstitial voids in the enclaves (Murphy et al., 1998), suggest that the
852 enclaves were intruded into the andesite as liquid blobs (e.g. Bacon, 1986; Clynne, 1999; Saito et al.,
853 2003). These textures however also indicate fairly rapid heat transfer and quenching, their high
854 vesicularity suggest that they may be permeable to gas flow and melt percolation. The small size of the
855 enclaves and short timescales (days to months) between reheating, mixing and eruption (Snyder, 2000;
856 Devine et al., 2003; Humphreys et al., 2010) will greatly restrict the volume of andesite that could be
857 contaminated by diffusion or advection from enclaves, and we reject this model based on time and
858 surface area constraints.
859
860
861

862 *Diffusion/advection from basal flow*

863 Due to the difference in density between the two magmas, basaltic injections into silicic chambers may
864 tend to occupy the base of the reservoir. Here the intricacies of the mixing could result in significant
865 hybridization of small volumes of silicic magma, trapped beneath the intruding mafic magma (e.g. Snyder
866 & Tait, 1995; 1998a; 1998b). Snyder & Tait (1998b) propose that isotopic and trace element signatures
867 can be transferred from basalt to andesite without significant effect on the major element chemistry apart
868 from FeO. This is achieved through a combination of diffusion and advection via the large surface area of
869 the fingered morphology created by the trapped andesite rising up through the overriding basalt due to
870 differences in density (Snyder & Tait, 1995; 1998a; Perugini & Poli, 2005).

871

872 Contamination of the andesite will increase its density due to water loss to the basalt and the migration of
873 FeO from the basalt to the andesite. The contaminated liquid thus forms a layer between the basalt and
874 uncontaminated andesite, in the same region where enclave formation is thought to occur (e.g.
875 Eichelberger, 1980; Thomas et al., 1993). The relatively higher temperature of the contaminated andesite
876 layer should delay quenching, thus giving more time for diffusion from the upper layer of the basalt.
877 The relatively higher density of the contaminated andesite liquid should make it easier for the basaltic
878 liquids to physically interact with and generate vesiculated blobs as enclaves into the contaminated
879 andesite (e.g. Thomas & Tait, 1997). Both compositions are subsequently erupted together as enclaves
880 and host andesite. Such a process would be consistent with the FeO content of the enclaves and their host
881 andesite lavas being coupled.

882

883 For a series of injections closely spaced in time, the process is repeated and any remnant contaminated
884 andesite liquids are further contaminated by the new influx. Subsequent basalt intrusions would create a
885 step like dispersal of the contaminants upwards via double diffusive convection. Rather than a rapid
886 dispersal via convection, trace element and isotopic gradients will be set up in the andesite as a function
887 of the number of injections encountered.

However if each injection leads to total extrusion of the contaminated liquid, the extruded andesite should have an imprint that is only controlled by the relative chemistry and volume of the basalt it encounters. There is no robust trace element and isotopic dataset for products erupted after Phase I, so we cannot test this model conclusively. However the migration of FeO from the basalt to the andesite as predicted by the model is consistent with our observations of the coupled FeO behaviour in both magmas and this therefore seems a good way to explain the behaviour of Fe in both magmas.

We previously highlighted a steady decrease in the gap between the Fe content of the andesite and the syn-erupted enclaves as the eruption progresses. This could be due to Fe-diffusion becoming more efficient with time. A second more plausible possibility is that residual liquids are being further contaminated over time by subsequent basalt influxes, and hence more efficient mixing may be occurring as the eruption proceeds due to the converging chemistries of the contaminated residue and the intruding basalt. We interpret the closing gap in relative bulk Fe contents as an indicator of further contamination of un-erupted previously contaminated andesite. This observation is consistent with a periodic basalt delivery into the andesite reservoir rather than a continuous trickle.

Gas fluxing

It has been demonstrated that the intruding basalt is the primary source of the SO_2 that is emitted from the Soufrière Hills volcano (Edmonds et al., 2001). The volcano has exhibited a type of behaviour termed as persistent degassing (Shinohara, 2008). Thus there has been a constant influx of volatiles into the andesite reservoir from the intruding basalt. The SO_2 flux through the andesite reservoir varies on timescales ranging from weeks to years and in most cases is independent of magma extrusion (Christopher et al., 2010). There is no evidence to indicate that the fluxing of volatiles through the andesitic system has a major influence on the andesitic groundmass composition.

Expected Future Trends and Behaviour

The changes in magma composition from Phase III onwards, coincide with an increase in the violence of activity during the extrusion phases. To date there is no strong evidence linking eruption style to magma composition during the eruption. However we expect subsequent extrusion phases during the present eruption to produce andesite and enclaves showing coupled Fe contents with both compositions showing similar inter-phase Fe trends. The Fe content of both magma types is further expected to converge due to the continued Fe enrichment from the repeated contamination of previously contaminated un-erupted andesite residue. We also expect the products of subsequent phases to show linear trends with little scatter.

Future Research

The variation in FeO content observed in the enclaves indicates significant changes in the basalt composition. It would be therefore useful to constrain the nature of basalt delivery into the andesite reservoir. Several petrogenetic processes are occurring contemporaneously during this eruption such as magma mixing, fractional crystallization, mafic recharge and possibly crustal contamination; all of which influence the magma compositions. The effects of each are poorly constrained and need to be deciphered by robust analysis of the trace element and isotopic geochemistry. The current trace element dataset is sparse and thus needs supplementing. Trace element and isotope data of the crystal cargo would also help better constrain the interaction between the basalt and andesite as well as any recharge episodes that would have occurred (e.g. Tonarini et al,. 1995; Browne et al., 2006; Davi et al., 2009).

Conclusions

i. Basaltic intrusion and the subsequent formation of mafic enclaves have played an integral role in eruptions at the Soufrière Hills volcano for millennia. The intruding basalt has been providing heat to the surrounding host andesite magma and hence energy for remobilizing the andesite throughout the current eruption.

ii. The early intruded basalt erupted in Phases I and II assimilated plutonic residue left over from previous basalt intrusions, while the basalt products of Phases III, IV and V encountered a relatively residue free reservoir floor.

iii. There are genuine inter-phase changes in the composition of the basalt arriving from depth, especially in the FeO content.

iv. Crystal fractionation of the basalt and subsequent mixing/mingling and diffusion produces a whole suite of hybrid magmas which are erupted as enclaves and host andesites; hence we are unable to sample the true composition of the intruded basalt or the pre intrusion andesite.

v. The andesites are likely hybridized by the basalt due to trapping of ambient andesite liquid beneath the basal intrusion which allows for diffusion and transfer of the basalt Fe signature to the andesite while it percolates upward through then resides on the basalt sheet. Transfer of elements such as Ca, Al and Mg are controlled predominantly by mixing and enclave destruction.

Acknowledgements

MCSH is supported by a Royal Society University Research Fellowship. We acknowledge assistance from Victoria Smith and Chiara Petrone during electron microprobe analysis as well as Crystal Mann for her helpful discussion. We also acknowledge the support of the British Geological Survey.

Appendix I - Possible inter-laboratory variability

The majority of bulk rock geochemical data collected and presented here for the first three phases of extrusion are from two main labs, Brown University (Joe Devine) and University of Leicester (Murphy and Sparks, 1999; Murphy et al., 2000; Zellmer et al., 2003a; MVO contract), with additional data from the labs at Bristol University, McGill University, British Geological Survey and University of East Anglia. To rule out laboratory bias as a source of the inter-phase FeO variation, we generated plots of FeO vs. SiO_2 for products from Phases I, II and III (Figure 11) demarcated by data source and eruption phase.

Despite some scatter, andesite analyses from a given eruptive phase overlap within error regardless of the laboratory used. For example, Phase II andesites clearly show reduced FeO contents relative to Phase I andesites while the Phase III andesites generally have lower FeO contents than Phase II andesites at similar SiO_2 (Figure 11a). The same pattern is true for the mafic enclaves where the Phase III products from two different labs have distinctly lower FeO contents (Figure 11b). To further investigate this, andesite and enclave splits from Phase I products were recently analyzed at the UEA lab and are included on the plot (Figure 11a & b). They show similar FeO contents to Phase I analyses from other labs (Figure 11a & b). We are therefore confident that the variations in Fe content are real and not a function of source laboratory. In addition, the correlation of FeO contents with other geochemical variables (e.g. trace elements such as Sc, Ba and V) indicates that these distinct FeO compositions are related to real differences in bulk rock compositions and not related to laboratory analysis.

References

ANDERSEN D. J., LINDSLEY D. H. & DAVIDSON P.M. 1993. QUILF: A pascal program to assess equilibria among Fe-Mg-Mn-Ti oxides, pyroxenes, olivine, and quartz. *Computers & Geosciences* **19**(9), 1333-1350.

ANDERSON D.J. & SMITH D.R. 1995. The effects of temperature and *f*O2 on the Al-hornblende barometer. *American Mineralogist* **80**, 549-559.

ARMIENTI P., TONARINI S., INNOCENTI F. & D' ORAZIO M. 2007. Mount Etna pyroxene as a tracer of petrogenetic processes and dynamics of the feeding system. *Geological Society of America Special Papers,* **418**, 265-276.

ASPINALL W. P., MILLER A. D., LYNCH L. L., LATCHMAN J. L., STEWART R. C., WHITE, R. A & POWER J. A.1998. Soufrière Hills Eruption, Montserrat, 1995-1997: Volcanic earthquake locations and fault plane solutions. *Geophysical Research Letters* **25** (18), 3397-3400.

BACHMANN O & DUNGAN M. A. 2002. Temperature-induced Al-zoning in hornblendes of the Fish Canyon magma, Colorado. *American Mineralogist* **87** (8-9), 1062-1076.

BACON C. R. 1986. Magmatic Inclusions in Silicic and Intermediate Volcanic-Rocks. *Journal of Geophysical Research-Solid Earth and Planets* **91**(B6), 6091-6112.

BARCLAY J., HERD R. A., EDWARDS B. R., CHRISTOPHER T.E., KIDDLE E. J., PLAIL M. & DONOVAN A. 2010. Caught in the act: Implications for the increasing abundance of mafic enclaves during the recent eruptive episodes of the Soufrière Hills Volcano, Montserrat. *Geophysical Research Letters* **37**, L00E09, doi:10.1029/2010GL042509.

BARCLAY J., RUTHERFORD M. J., CARROLL M. R., MURPHY M. D., DEVINE J. D., GARDNER J. & SPARKS R. S. J. 1998. Experimental phase equilibria constraints on pre-eruptive storage conditions of the Soufrière Hills magma. *Geophysical Research Letters* **25**(18), 3437-3440.

BÈDARD J.H. 2010. Parameterization of the Fe=Mg exchange coefficient (Kd) between clinopyroxene and silicate melts. *Chemical Geology,* **274** (3-4), 169-176.

BLUNDY J., CASHMAN K. & HUMPHREYS, M.C.S. 2006. Magma heating by decompression-driven crystallization beneath andesite volcanoes. *Nature* **443**(7107) 76-80.

BLUNDY J. D. & HOLLAND T. J. B. 1990. Calcic Amphibole Equilibria and a New Amphibole-Plagioclase Geothermomemeter. *Contributions to Mineralogy and Petrology* **104**(2) 208-224.

BOLGE L.L., CARR M.J., FEIGENSON M.D. & ALVARADO G.E. 2006. Geochemical stratigraphy and magmatic evolution at Arenal Volcano, Costa Rica. *Journal of Volcanology and Geothermal Research* **157** (1-3), 34-48.

BROWNE B.L., EICHELBERGER J.C. PATINO L.C., VOGEL T.A., UTO K. & HOSHIZUMI H. 2006. Magma mingling as indicated by texture and Sr/Ba ratios of plagioclase phenocrysts from Unzen volcano, SW Japan. *Journal of Volcanology and Geothermal Research* **154**(1-2) 103-116.

BUCKLEY V., SPARKS R. & WOOD B. 2006. Hornblende dehydration reactions during magma ascent at Soufrière Hills Volcano, Montserrat. *Contributions to Mineralogy and Petrology* **151**, 121-140.

CALDER E. S., LUCKETT R., SPARKS R. S. J & VOIGHT B. 2002. Mechanisms of lava dome instability and generation of rock falls and pyroclastic flows at Soufrière Hills Volcano, Montserrat. *Geological Society, London, Memoir*, **21** (1)173-190.

CASHMAN K. V. 1992. Groundmass crystallization of Mount St. Helens dacite, 1980-1986: a tool for interpreting shallow magmatic processes. *Contributions to Mineralogy and Petrology* **109**, 431-449.

CHRISTOPHER T.E., EDMONDS M., HUMPHREYS M. C. S. & HERD R. A.2010. Volcanic gas emissions from Soufrière Hills Volcano, Montserrat 1995-2009, with implications for mafic magma supply and degassing. *Geophysical Research Letters* **37**, L00E04, doi: 10.1029/2009GL041325

CLYNNE M. A. 1999. A Complex Magma Mixing Origin for Rocks Erupted in 1915, Lassen Peak, California. *Journal of Petrology* **40**(1), 105-132.

COUCH S., HARFORD C. L., SPARKS R. S. J. & CARROLL M. R. 2003a. Experimental Constraints on the Conditions of Formation of Highly Calcic Plagioclase Microlites at the Soufrire Hills Volcano, Montserrat. *Journal of Petrology* **44**(8), 1455-1475.

COUCH S., SPARKS R. S. J. & CARROLL M. R. 2003b. The Kinetics of Degassing-Induced Crystallization at Soufrière Hills Volcano, Montserrat. *Journal of Petrology* **44**(8), 1477-1502.

DAVI M., BEHRENS H., VETERE F. & DE ROSA R. 2009. The viscosity of latitic melts from Lipari (Aeolian Islands, Italy): Inference on mixing-mingling processes in magmas. *Chemical Geology* **259**(1-2), 89-97.

DEVINE J. D., GARDNER J. E., BRACK H. P., LAYNE G. D. & RUTHERFORD M. J. 1995. Comparison of Microanalytical Methods for Estimating H_2O Contents of Silicic Volcanic Glasses. *American Mineralogist* **80**(3-4), 319-328.

DEVINE J. D., MURPHY M. D., RUTHERFORD M. J., BARCLAY J., SPARKS R. S. J., CARROLL M. R., YOUNG S. R. & GARDNER J. E. 1998a. Petrologic evidence for pre-eruptive pressure-temperature conditions, and recent reheating, of andesitic magma erupting at the Soufrière Hills Volcano, Montserrat, WI. *Geophysical Research Letters* **25**(19), 3669-3672.

DEVINE J. D., RUTHERFORD M. J. & GARDNER J. E. 1998b. Petrologic determination of ascent rates for the 1995-1997 Soufrière Hills Volcano andesitic magma. *Geophysical Research Letters* **25**(19), 3673-3676.

DEVINE J. D., RUTHERFORD M. J., NORTON G. E. & YOUNG S. R. 2003. Magma Storage Region Processes Inferred from Geochemistry of Fe-Ti Oxides in Andesitic Magma, Soufrière Hills Volcano, Montserrat, W.I. *Journal of Petrology* **44**(8), 1375-1400.

DEVINE J. D. & RUTHERFORD M. J. this volume. Magma Storage Processes of the Soufrière Hills Volcano Montserrat W.I. *Geological Society of London Memoir*, (The eruption of Soufrière Hills Volcano, Montserrat from 2000 to 2010).

DUPUY C., DOSTAL J. & TRAINEAU H.1985. Geochemistry of volcanic rocks from Mt. Pelée, Martinique. *Journal of Volcanology and Geothermal Research **26*** (1-2), 147-165.

EDMONDS M., HUMPHREYS M.C.S., HARUI E., HERD R., WADGE G., RAWSON H., LEDDEN R., PLAIL M., BARCLAY J., AIUPPA A., CHRISTOPHER T.E., GIUDICE G. & GUIDA R. 2013. Pre-eruptive vapour and its role in controlling eruption style and longevity at Soufrière Hills Volcano. *Geological Society of London Memoir*, (The eruption of Soufrière Hills Volcano, Montserrat from 2000 to 2010).

EDMONDS M., HERD R.A. & STRUTT M.H. 2006. Tephra deposits associated with a large lava dome collapse, Soufrière Hills Volcano, Montserrat, 12-15 July 2003. *Journal of Volcanology and Geothermal Research* **153** (3-4), 313-330.

EDMONDS M., PYLE D. & OPPENHEIMER C.2001. A model for degassing at the Soufrière Hills Volcano, Montserrat, West Indies, based on geochemical data. *Earth and Planetary Science Letters* **186** (2), 159-173.

EDWARDS B. R. & RUSSELL J. K. 1998. Time scales of magmatic processes: New insights from dynamic models for magmatic assimilation *Geology* **26** (12), 1103-1106.

EICHELBERGER J. C. 1980. Vesiculation of Mafic Magma During Replenishment of Silicic Magma Reservoirs. *Nature* **288**(5790), 446-450.

ELSWORTH D., MATTIOLI G., TARON J., VOIGHT B. & HERD R. 2008. Implications of Magma Transfer between Multiple Reservoirs on Eruption Cycling. Science **322** (5899), 246-248.

ERNST W. G. & LIU J. 1998. Experimental phase-equilibrium study of Al- and Ti-contents of calcic amphibole in MORB - A semiquantitative thermobarometer. *American Mineralogist* **83**(9-10), 952-969.

FICHAUT M., MARCELOT G. & CLOCCHIATTI R. 1989a. Magmatology of Mt. Pelée (Martinique, F.W.I.). II: Petrology of gabbroic and dioritic cumulates. *Journal of Volcanology and Geothermal Research* **38**(1-2), 171-187.

FICHAUT M., MAURY R.C., TRAINEAU H., WESTERCAMP D., JORON J.L., GOURGAUD A. & COULON C. 1989b. Magmatology of Mt. Pelée (Martinique, F.W.I.). III: Fractional crystallization versus magma mixing. *Journal of Volcanology and Geothermal Research* **38**(1-2), 189-213.

FOROOZAN R., ELSWORTH D., VOIGHT B. & MATTIOLI G. S. 2010. Dual reservoir structure at Soufrière Hills Volcano inferred from continuous GPS observations and heterogeneous elastic modeling. Geophysical Research Letters **37** L00E12, doi: 10.1029/2010GL042511.

FOROOZAN R., ELSWORTH D., VOIGHT B. & MATTIOLI G. S. 2011. Magmatic-metering controls the stopping and restarting of eruptions. *Geophysical Research Letters* **38**, L05306, doi: 10.1029/2010GL046591.

GARCIA M. O. & JACOBSON S. S. 1979. Crystal clots, amphibole fractionation and the evolution of calc-alkaline magmas. *Contributions to Mineralogy and Petrology* **69**, 319-327.

GENAREAU K. & CLARKE A. B. 2010. Heterogeneous clasts as windows into magma mingling at Soufrière Hills volcano. *Geophysical Research Letters* **37**, L00E02, doi:10.1029/2009GL041968.

GOURGAUD A., FICHAUT M. & JORON J.L.1989. Magmatology of Mt. Pelee(Martinique, F.W.I.). I: Magma mixing and triggering of the 1902 and 1929 Pelean nuees ardentes. *Journal of Volcanology and Geothermal Research* **38** (1-2), 143-169.

GRASSET O. & ALBAREDE F. 1994. Hybridization of mingling magmas with different densities. *Earth and Planetary Science Letters* **121**(3-4), 327-332.

HAMMARSTROM J. M. & ZEN E. A. 1986. Aluminum in Hornblende - an Empirical Igneous Geobarometer. *American Mineralogist* **71**(11-12), 1297-1313.

HAMMER J. E. & RUTHERFORD M. J. 2002. An experimental study of the kinetics of decompression-induced crystallization in silicic melt. *Journal of Geophysical Research* **107**(B1), 2021.

HERD R.A., EDMONDS M. & BASS V. A. 2005. Catastrophic lava dome failure at Soufrière Hills Volcano, Montserrat, 12-13 July 2003. *Journal of Volcanology and Geothermal Research* **148** (3-4), 234-252.

HIGGINS M. D. & ROBERGE J. 2003. Crystal Size Distribution of Plagioclase and Amphibole from Soufrière Hills Volcano, Montserrat: Evidence for Dynamic Crystallization-Textural Coarsening Cycles. *Journal of Petrology* **44**(8), 1401-1411.

HOLLISTER L. S., GRISSOM G. C., PETERS E. K., STOWELL H. H. & SISSON V. B. 1987. Confirmation of the Empirical Correlation of Al in Hornblende with Pressure of Solidification of Calc-Alkaline Plutons. *American Mineralogist* **72**(3-4), 231-239.

HUMPHREYS M. C. S., CHRISTOPHER T.E. & HARDS V. 2009a. Microlite transfer by disaggregation of mafic inclusions following magma mixing at Soufrière Hills volcano, Montserrat. *Contributions to Mineralogy and Petrology* **157**(5), 609-624.

HUMPHREYS M. C. S., EDMONDS M., BARCLAY J., PLAIL M., PARKES D. & CHRISTOPHER T.E. 2013. A new method to quantify the real supply of mafic components to a hybrid andesite. *Contributions to Mineralogy and Petrology* **165**, 191-215

HUMPHREYS M. C. S., EDMONDS M., CHRISTOPHER T.E. & HARDS V. 2009b. Chlorine variations in the magma of Soufrière Hills Volcano, Montserrat: Insights from Cl in hornblende and melt inclusions. *Geochimica et Cosmochimica Acta* **73**(19), 5693-5708.

HUMPHREYS M. C. S., EDMONDS M., CHRISTOPHER T.E. & HARDS V. 2010. Magma hybridisation and diffusive exchange recorded in heterogeneous glasses from Soufrière Hills Volcano, Montserrat. *Geophysical Research Letters* **37**, L00E06, doi: 10.1029/2009GL041926.

HUMPHREYS M. C. S., KEARNS S.L. & BLUNDY J.D. 2006. SIMS investigation of electron-beam damage to hydrous, rhyolitic glasses: Implications for melt inclusion analysis. *American Mineralogist* **91**(4), 667-679.

JOHNSON M. C. & RUTHERFORD M.J. 1989. Experimental Calibration of the Aluminum-in-Hornblende Geobarometer with Application to Long-Valley Caldera (California) Volcanic-Rocks. *Geology* **17**(9), 837-841.

KOMOROWSKI J. C., LEGENDRE Y., CHRISTOPHER T.E., BERNSTEIN M., STEWART R., JOSEPH E., FOURNIER N., CHARDOT L., FINIZOLA A., WADGE G., SYERS R., WILLIAMS C. & BASS V. 2010. Insights into processes and deposits of hazardous vulcanian explosions at Soufrière Hills Volcano during 2008 and 2009 (Montserrat, West Indies). *Geophysical Research Letters* **37**, L00E19,doi:10.1029/2010GL042558.

KUSHIRO I. 1960. Si-Al relation in clinopyroxenes from igneous rocks. *American Journal of Science*. **258** (8), 548-554.

LINDSLEY D. H. (1983). Pyroxene Thermometry. *American Mineralogist* **68**(5-6), 477-493.

MARTEL C., RADADI A.A., POUSSINEAU S., GOURGAUD A. & PICHAVANT M. 2006. Basalt-inherited microlites in silicic magmas: Evidence from Mount Pelée (Martinique, French West Indies). *Geology* **34** (11), 905-908.

MILLER A. D., STEWART R. C., WHITE R. A., LUCKETT R., BAPTIE B. J., ASPINALL W. P., LATCHMAN J. L., LYNCH L. L. & VOIGHT B. 1998. Seismicity associated with dome growth and collapse at the Soufrière Hills Volcano, Montserrat. *Geophysical Research Letters* **25** (18), 3401-3404.

MURPHY M. D., SPARKS R. S. J., BARCLAY J., CARROLL M. R. & BREWER T. S. 2000. Remobilization of andesite magma by intrusion of mafic magma at the Soufrière Hills Volcano, Montserrat, West Indies. *Journal of Petrology* **41**(1), 21-42.

MURPHY M. D., SPARKS R. S. J., BARCLAY J., CARROLL M. R., LEJEUNE A. M., BREWER T. S., MACDONALD R., BLACK S. & YOUNG S. 1998. The role of magma mixing in triggering the current eruption at the Soufrière Hills volcano, Montserrat, West Indies. *Geophysical Research Letters* **25**(18), 3433-3436.

NEWMAN S. & LOWENSTERN J.B. 2002. VolatileCalc: a silicate melt-H_2O-CO_2 solution model written in Visual Basic for excel. Computers & Geosciences **28**(5), 597-604.

NORTON G. E., WATTS R. B., VOIGHT B., MATTIOLI G. S., HERD R. A., YOUNG S. R., DEVINE J.D., ASPINNALL W. P., BONADONNA C., BAPTIE B. J., EDMONDS M., JOLLY A. D., LOUGHLIN S. C., LUCKETT R. & SPARKS S. J. 2002. Pyroclastic flow and explosive activity at Soufrière Hills Volcano, Montserrat, during a period of virtually no magma extrusion (March 1998 to November 1999). *Geological Society, London, Memoir* **21** (1), 467-481.

ODBERT H.M., STEWART R.C. & WADGE G. this volume. Cyclic Phenomena at the Soufrière Hills Volcano, Montserrat. *Geological Society of London Memoir*, (The eruption of Soufrière Hills Volcano, Montserrat from 2000 to 2010).

PERUGINI D. & POLI G.2005. Viscous fingering during replenishment of felsic magma chambers by continuous inputs of mafic magmas: Field evidence and fluid-mechanics experiments. *Geology* **33** (1), 5-8.

PICHAVANT M., COSTA F., BURGISSER A., SCAILLET B., MARTEL C. & POUSSINEAU S. 2007. Equilibration Scales in Silicic to Intermediate Magmas-Implications for Experimental Studies. *Journal of Petrology* **48** (10), 1955-1972.

PICHAVANT M., MARTEL C., BOURDIER J.L. & SCAILLET B. 2002. Physical conditions, structure, and dynamics of a zoned magma chamber: Mount Pelée (Martinique, Lesser Antilles Arc). Journal of Geophysical Research: Solid Earth. **105 B5**, doi - 10.1029/2001JB000315.

PLAIL M., BARCLAY J., HUMPHREYS M. C. S., EDMONDS M., HERD R.A. & CHRISTOPHER T.E. this volume. Characterisation of mafic enclaves in the erupted products of Soufrière Hills Volcano, Montserrat 1995-2010. *Geological Society of London Memoir*, (The eruption of Soufrière Hills Volcano, Montserrat from 2000 to 2010).

PLECHOV P., TSAI A., SHCHERBAKOV V. & DIRKSEN O. 2008. Opacitization conditions of hornblende in Bezymyannyi volcano andesites (March 30, 1956 eruption). *Petrology* **16** (1), 19-35.

PUTIRKA K.D. 1999. Clinopyroxene plus liquid equilibria to 100 kbar and 2450 K. *Contributions to Mineralogy and Petrology* **135**(2-3), 151-163.

PUTIRKA K. D. 2005. Igneous thermometers and barometers based on plagioclase + liquid equilibria: Tests of some existing models and new calibrations. *American Mineralogist* **90**(2-3), 336-346.

PUTIRKA K.D., JOHNSON M., KINZLER R., LONGHI J. & WALKER D. 1996. Thermobarometry of mafic igneous rocks based on clinopyroxene-liquid equilibria, 0-30 kbar. *Contributions to Mineralogy and Petrology* **123**(1), 92-108.

PUTIRKA K. D., MIKAELIAN H., RYERSON F. & SHAW H. 2003. New clinopyroxene-liquid thermobarometers for mafic, evolved, and volatile-bearing lava compositions, with applications to lavas from Tibet and the Snake River Plain, Idaho. *American Mineralogist* **88**(10), 1542-1554.

REAGAN M. K., GILL J.B., MALAVASSI E. & GARCIA M.O. 1987. Changes in magma composition at Arenal volcano, Costa Rica, 1968-1985: Real-time monitoring of open-system differentiation. *Bulletin of Volcanology* **49**, 415-434.

RHODES J.M. & DUNGAN M.A. 1977. The nature of primary ocean floor basalts. Papers presented to the second inter-team meeting, *Basaltic volcanism study project*. 50-52. Lunar Science Institute, Huston.

RIDOLFI F., RENZULLI A. & PUERINI M. 2010. Stability and chemical equilibrium of amphibole in calc-alkaline magmas: an overview, new thermobarometric formulations and application to subduction-related volcanoes. *Contributions to Mineralogy and Petrology* **160**(1), 45-66.

ROBERTSON R. E. A., ASPINALL W. P., HERD R. A., NORTON G. E., SPARKS R. S. J. & YOUNG, S. R. 2000. The 1995-1998 eruption of the Soufrière Hills volcano, Montserrat, WI. *Philosophical Transactions of the Royal Society of London Series A-Mathematical Physical and Engineering Sciences* **358** (1770) 1619-1637.

RUTHERFORD M. J. & DEVINE J. D. 2003. Magmatic Conditions and Magma Ascent as Indicated by Hornblende Phase Equilibria and Reactions in the 1995-2002 Soufrière Hills Magma. *Journal of Petrology* **44**(8), 1433-1453.

RUTTER M. J., VANDERLAAN S. R. & WYLLIE P. J. 1989. Experimental-Data for a Proposed Empirical Igneous Geobarometer - Aluminum in Hornblende at 10 Kbar Pressure. *Geology* **17**(10): 897-900.

RYDER C.H., GILL J.B., TEPLEY III F., RAMOS F. & REAGAN M. 2006. Closed- to open-system differentiation at Arenal volcano (1968-2003). *Journal of Volcanology and Geothermal Research* **157** (1-3), 75-93.

SAITO G., KOHEI K. & HIROSHI S. 2003. Volatile evolution of Satsuma-Iwojima volcano: Degassing process and mafic-felsic magma interaction. *Developments in Volcanology Melt Inclusions in Volcanic Systems - Methods, Applications and Problems* **5**, 129-146.

SCHMIDT M. W. 1992. Amphibole composition in tonalite as a function of pressure: an experimental calibration of the Al-in-hornblende barometer. *Contributions to Mineralogy and Petrology* **110**(2), 304-310.

SCHUMACHER J. C. 1997. The estimation of ferric iron in electron microprobe analysis of amphiboles. *Mineralogical Magazine* **61**, 312-321.

SHEPHERD J., TOMBLIN J. & WOO D.1971. Volcano-seismic crisis in Montserrat, West Indies, 1966-67. *Bulletin of Volcanology* **35**, 143-162.

SHINOHARA H.2008. Excess Degassing from Volcanoes and Its Role on Eruptive and Intrusive Activity. *Reviews of Geophysics* **46** (4). WOS:000260997900001.

SNYDER D. 2000. Thermal effects of the intrusion of basaltic magma into a more silicic magma chamber and implications for eruption triggering. *Earth and Planetary Science Letters* **175**(3-4), 257-273.

SNYDER D. & TAIT S. 1995. Replenishment of magma chambers: comparison of fluid-mechanic experiments with field relations. *Contributions to Mineralogy and Petrology* **122** (3), 230-240.

SNYDER, D. & TAIT S. 1998a. A flow-front instability in viscous gravity currents. *Journal of Fluid Mechanics* **369**, 1-21.

SNYDER, D. & TAIT S. 1998b. The imprint of basalt on the geochemistry of silicic magmas. *Earth and Planetary Science Letters* **160**(3-4), 433-445.

SPARKS, R. S. J. & MARSHALL L. A. 1986. Thermal and mechanical constraints on mixing between mafic and silicic magmas. *Journal of Volcanology and Geothermal Research* **29**(1-4), 99-124.

STINTON A.J., COLE P. D., ODBERT H.M., CHRISTOPHER T.E, AVARD G. & BERNSTEIN M. 2013. Evolution of the Soufrière Hills volcano during a short, intense episode of dome growth: 4 October 2009 - 11 February 2010. *Geological Society of London Memoir*, (The eruption of Soufrière Hills Volcano, Montserrat from 2000 to 2010).

STORMER J. C. 1983. The Effects of Recalculation on Estimates of Temperature and Oxygen Fugacity from Analyses of Multicomponent Iron Titanium-Oxides. *American Mineralogist* **68**(5-6), 586-594.

STRECK M., DUNGAN M., MALAVASSI E. M., REAGAN M. & BUSSY F. 2002. The role of basalt replenishment in the generation of basaltic andesites of the ongoing activity at Arenal volcano, Costa Rica: evidence from clinopyroxene and spinel. *Bulletin of Volcanology* **64** (5), 316-327.

THOMAS N. & TAIT S.R. 1997. The dimensions of magmatic inclusions as a constraint on the physical mechanism of mixing. *Journal of Volcanology and Geothermal Research* **75** (1-2), 167-178.

THOMAS N., TAIT S. & KOYAGUCHI T. 1993. Mixing of stratified liquids by the motion of gas bubbles: application to magma mixing. *Earth and Planetary Science Letters* **115**(1-4), 161-175.

TONARINI S., ARMIENTI P., D'ORAZIO M., INNOCENTI F., POMPILIO M. & PETRINI R. 1995. Geochemical and isotopic monitoring of Mt Etna 1989-1993 eruptive activity: bearing on the shallow feeding system. *Journal of Volcanology and Geothermal Research,* **64**, 95-115.

TRAIL A. F. & SPERA F.J. 1990. Mechanisms for the generation of compositional heterogeneities in magma chambers. *Geological Society of America Bulletin* **102** (3), 353-367.

WADGE G., HERD R., RYAN G., CALDER E. S. & KOMOROWSKI J.C. 2010. Lava production at Soufrière Hills Volcano, Montserrat: 1995-2009. *Geophysical. Research Letters* **37**, doi- 10.1029/2009GL041466.

WADGE G. & ISAACS M. C. 1988. Mapping the Volcanic Hazards from Soufrière Hills Volcano, Montserrat, West Indies Using an Image Processor. *Journal of the Geological Society* **145**, 541-552.

YOUNG S., SPARKS R.S.J., ASPINALL W.P., LYNCH L.L., MILLER A.D., ROBERTSON R.E.A. & SHEPHERD J.B. 1998. Overview of the eruption of Soufrière Hills Volcano, Montserrat, 18 July 1995 to December 1997. *Geophysical. Research Letters* **25** (18) 3389-3392.

ZELLMER G. F., HAWKESWORTH C. J., SPARKS R. S. J., THOMAS L. E., HARFORD C. L., BREWER T. S. & LOUGHLIN S. C. 2003a. Geochemical Evolution of the Soufrière Hills Volcano, Montserrat, Lesser Antilles Volcanic Arc. *Journal of Petrology* **44**(8), 1349-1374.

ZELLMER G. F., SPARKS R.S.J., HAWKESWORTH C. J. & WIEDENBECK M. 2003b. Magma Emplacement and Remobilization Timescales Beneath Montserrat: Insights from Sr and Ba Zonation in Plagioclase Phenocrysts. *Journal of Petrology* **44**(8), 1413-1431.

Figure captions

Figure 1 Box plots showing relative plagioclase An contents by eruption phase for andesite phenocryst rims A, andesite microlites B, sieved rims, oscillatory rims and enclave crystals C, phenocryst cores by texture D. Microlite Fe content vs An content by phase E, Fe content vs An content for sieve and enclave crystals F.

Figure 2 Typical andesite whole rock texture found in Phases IV and V. pl – plagioclase, px- orthopyroxene, cpx- clinopyroxene, ox- Fe-Ti oxide.

Figure 3 Examples of enclave textures described by Plail et al (this volume). P- plagioclase, Px – clinopyroxene, Hbl – hornblende, Ox – Fe-Ti oxides, V – vesicles

Figure 4 Amphibole compositions in andesite and enclaves by phase A, box plots for mg#'s of amphibole phenocryst rims in the andesite B, enclaves by phase and mg# C, enclaves by phase and Fe content D. an- andesite, en- enclaves. The number of analyses used is given in each box, horizontal line represents median values.

Figure 5 Box plots of mg# for andesite orthopyroxene unzoned rims (by phase) and rev-zoned rims A, andesite orthopyroxene microlites (by phase) and enclave microlites B, bulk rock total alkali by eruption phase C, andesite hosted clinopyroxene microlite Kd values by phase D. The number of analyses used is given in each box, horizontal line represents median values. an – andesites, en- enclaves.

Figure 6 Abundances of major elements in andesite and enclave glass from microprobe analyses, andesites- An, enclaves- En. High $K_2O > 3$wt%, low $K_2O < 3$wt%.

Figure 7 Bulk andesite and enclave major element abundances by phase, vertical dashed line demarcates boundary between silica content of the andesite- An, enclave- En.

Figure 8 Box plots showing inter-phase bulk rock contents of FeO, V, Ba and plagioclase microlite Fe content throughout the eruption. The number of analyses used is given in each box, horizontal line represents median values, mic- microlite, an – andesites, en- enclaves.

Figure 9 Selected trace element plots for bulk rock andesite and enclave products. Symbols and labels are the same as Figure 7, vertical line demarcates boundary between andesite and enclave silica content.

Figure 10 Major element behaviour with changing FeO/MgO showing changes as function of crystal control. Arrows indicate removal of particular mineral phase. An- andesite, En – enclaves. Fractionation and assimilation vectors for the other oxides are same as in Al_2O_3.

Figure 11 Harker plots of SiO_2 vs FeO for phases 1, II and III by lab showing an absence of any systematic inter-lab variation in the data for andesites- A and enclaves-B. L-leciester, JD- Joe Devine, SS- (Murphy et al., 1998), BGS- British geological survey, UEA- University of East Anglia, MGU- Mc Gill University.

Table captions

Table 1 Laboratory and sample information for the XRF data used in this study; An-andesite, En- enclave.

Table 2 Published modal mineral contents for the first three extrusion phases. Arbitrary distinction between microlites and microphenocryst defined by 100μm, *Recalculated from point counts in Humphreys et al., 2009a, range shown.

Table 3 Mineral phases and associated textures in the andesite and enclave lavas of the current eruption.

Table 4 Averaged andesite plagioclase phenocryst and microlite microprobe data, comparing compositions from Phases IV and V with the published compositions of Phases I, II and III. pc- phenocryst core, pr - phenocryst rim, mc- microlite core, mr- microlite rim, mpc- microphenocryst core, mpr – microphenocryst rim, An- andesite, En – enclave.

Table 5a Averaged andesite amphibole compositions by texture and eruption phase.

Table 5b Averaged enclave amphibole compositions from eruption Phases I, II, III and V along side high aluminum andesite hosted microphenocrysts and groundmass fragments. Mphx – microphenocrysts, Frag – groundmass fragments. Phase V data from Plail et al. (this volume)

Table 6a Averaged Orthopyroxene phenocryst and microlite compositions comparing the andesite crystals of phase IV and V with crystals from phases I, II and III , errors are ± 1σ, mic – microlites, phx- phenocrysts.

Table 6b Averaged compositions of andesite hosted reverse zoned orthopyroxene phenocryst rims along with andesite and enclave microphenocrysts, errors are ± 1σ, Mphx- microphenocrysts, Phx- phenocrysts

Table 6c Averaged compositions of clinopyroxene microphenocrysts, microlites and overgrowths, errors are ± 1σ, mic – microlites, mphx- microphenocrysts.

Table 7a Averaged andesite titanomagnetite compositions, sorted by eruptive phase and textural type. Usp/Ilm mol% after Stormer (1983), mic – microlites.

Table 7b Averaged compositions of enclave oxides along with andesite derived ilmenite.

Table 8 Averaged microprobe glass compositions for andesites and enclaves, along with log *f*o2 values from touching ilmenite–magnetite pairs.

Table 9 Averaged bulk rock major element compositions for the andesite and enclaves of the different eruption phases.

Table 10 Averaged bulk rock trace element for andesites and enclaves of the different eruption phases.

Table 11 Temperature and Pressure estimates for the eruptive products obtained using a number of different techniques.

1484 Table 12 Intra-phase andesite mass balance calculations for addition of enclave crystals, weight % values
1485 are relative to initial magma compositions.

1486

1487

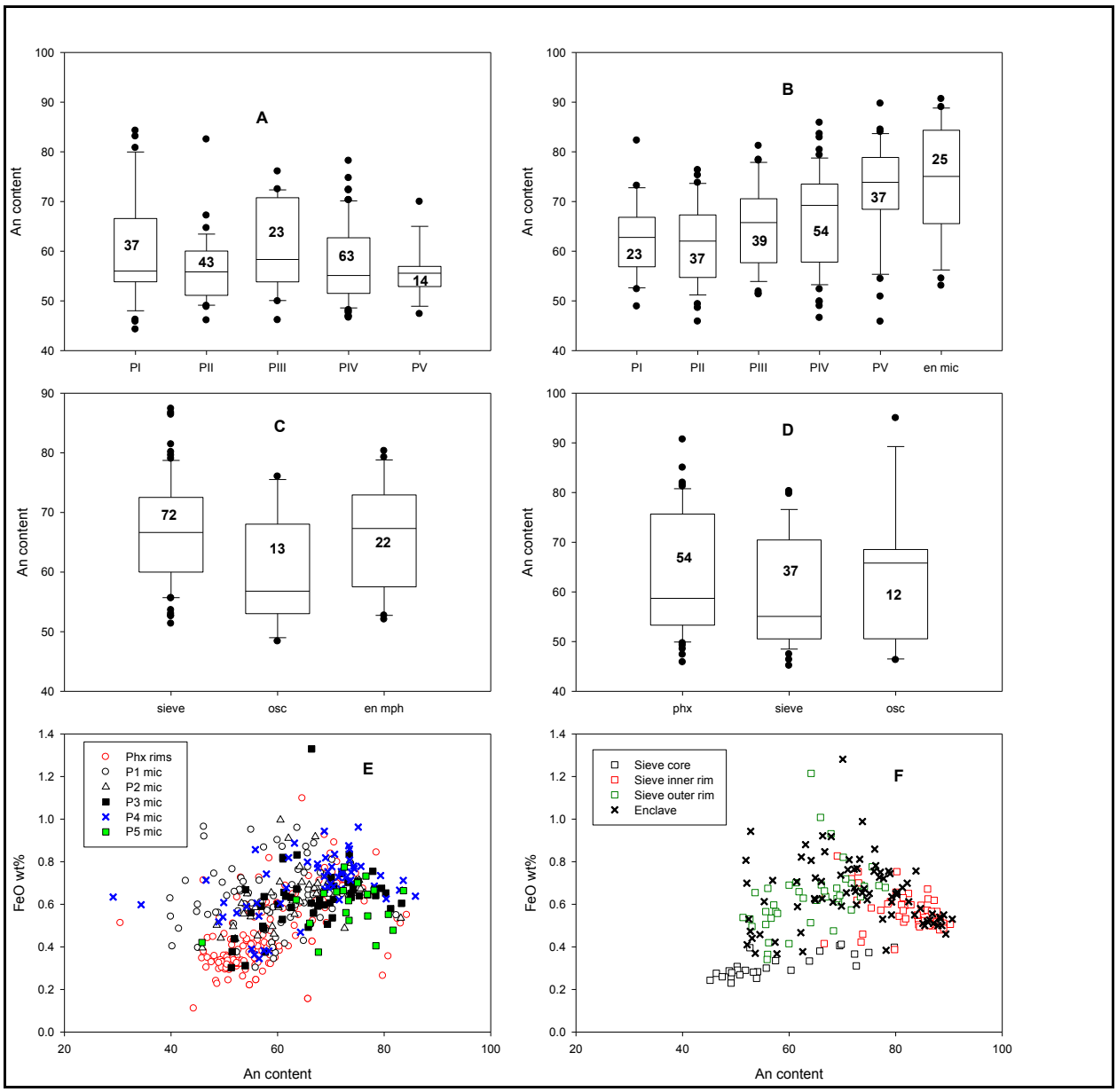

Figure 1 Box plots showing relative plagioclase An contents by eruption phase for andesite phenocryst rims A, andesite microlites B, sieved rims, oscillatory rims and enclave crystals C, phenocryst cores by texture D. Microlite Fe content vs An content by phase E, Fe content vs An content for sieve and enclave crystals F.

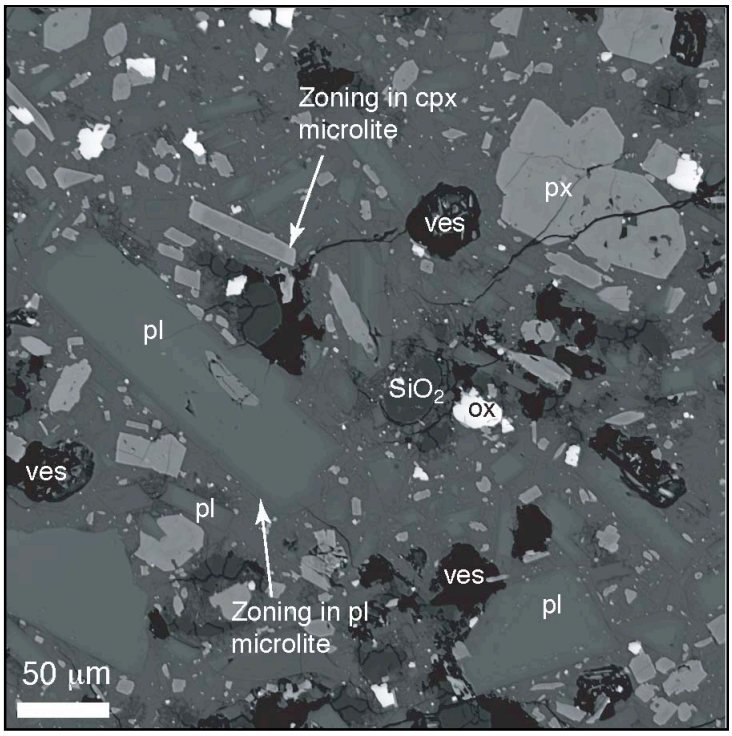

Figure 2 Typical andesite whole rock texture found in Phases IV and V.

pl – plagioclase, px- orthopyroxene, cpx- clinopyroxene, ox- Fe-Ti oxide.

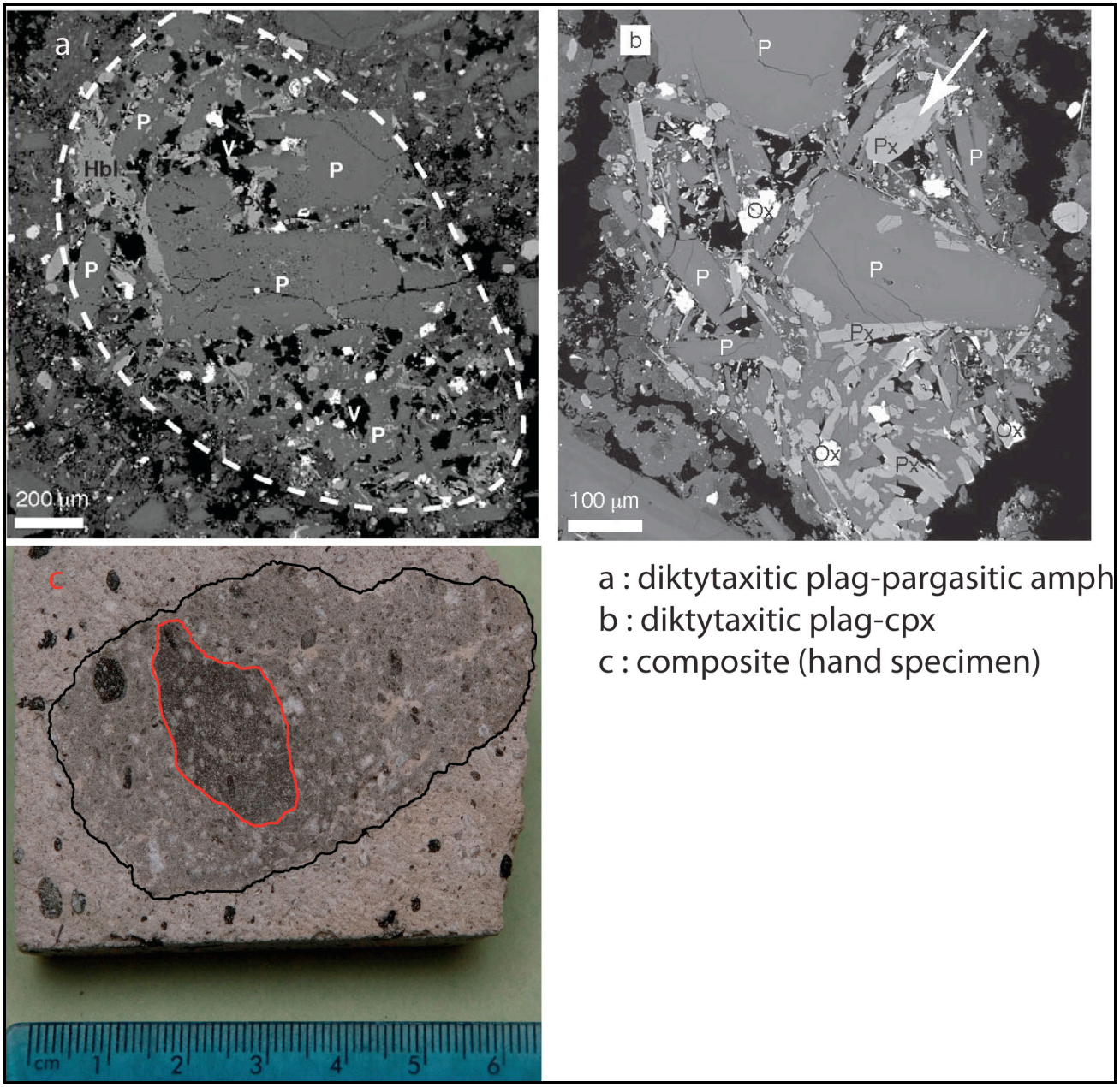

Figure 3 Examples of enclave textures described by Plail et al (this volume). P- plagioclase, Px – clinopyroxene, Hbl – horneblende, Ox – Fe-Ti oxides, V – vesicles

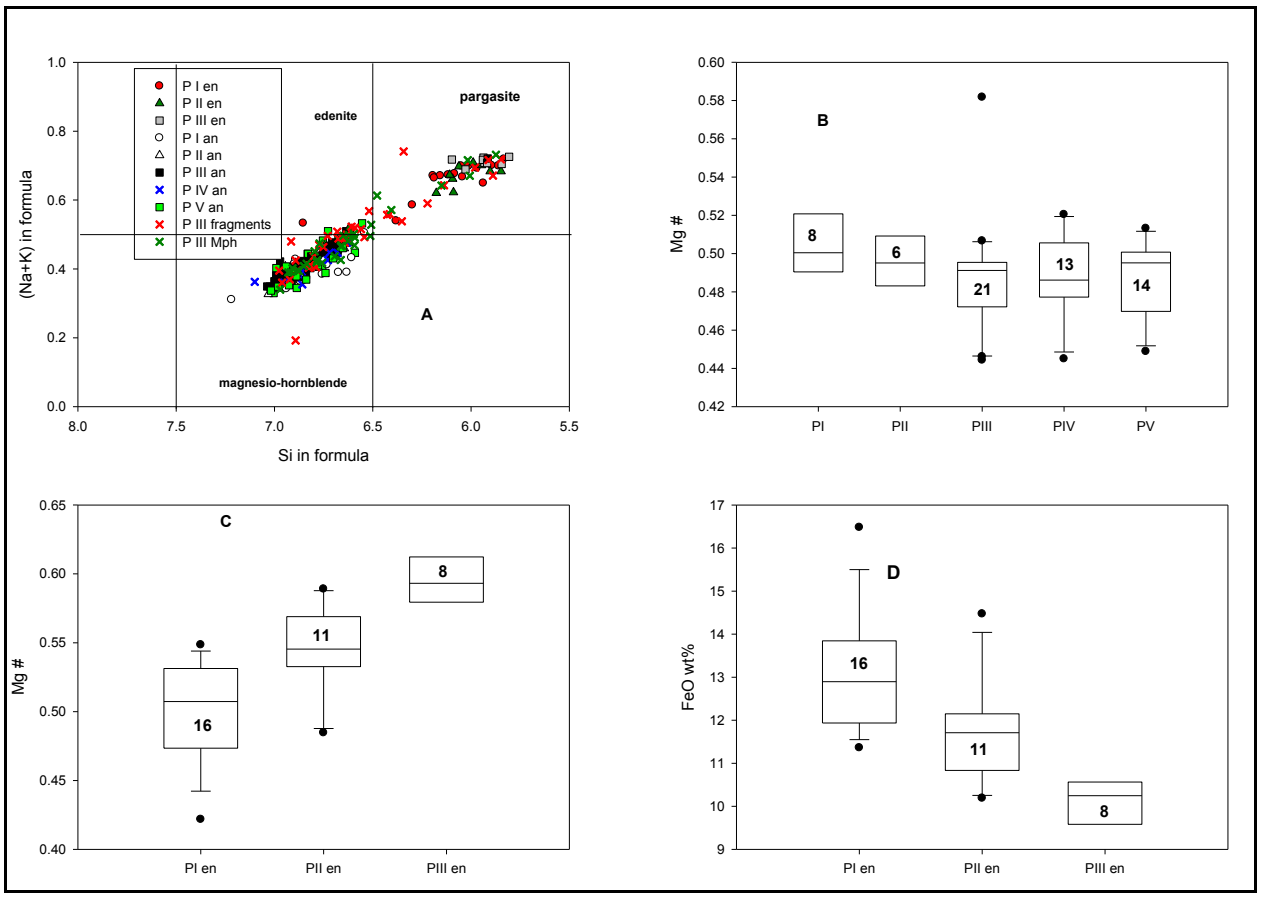

Figure 4 Amphibole compositions in andesite and enclaves by phase A, box plots for mg#s of amphibole phenocryst rims in the andesite B, enclaves by phase and mg# C, enclaves by phase and Fe content D. an-andesite, en- enclaves. The number of analyses used is given in each box, horizontal line represents median values.

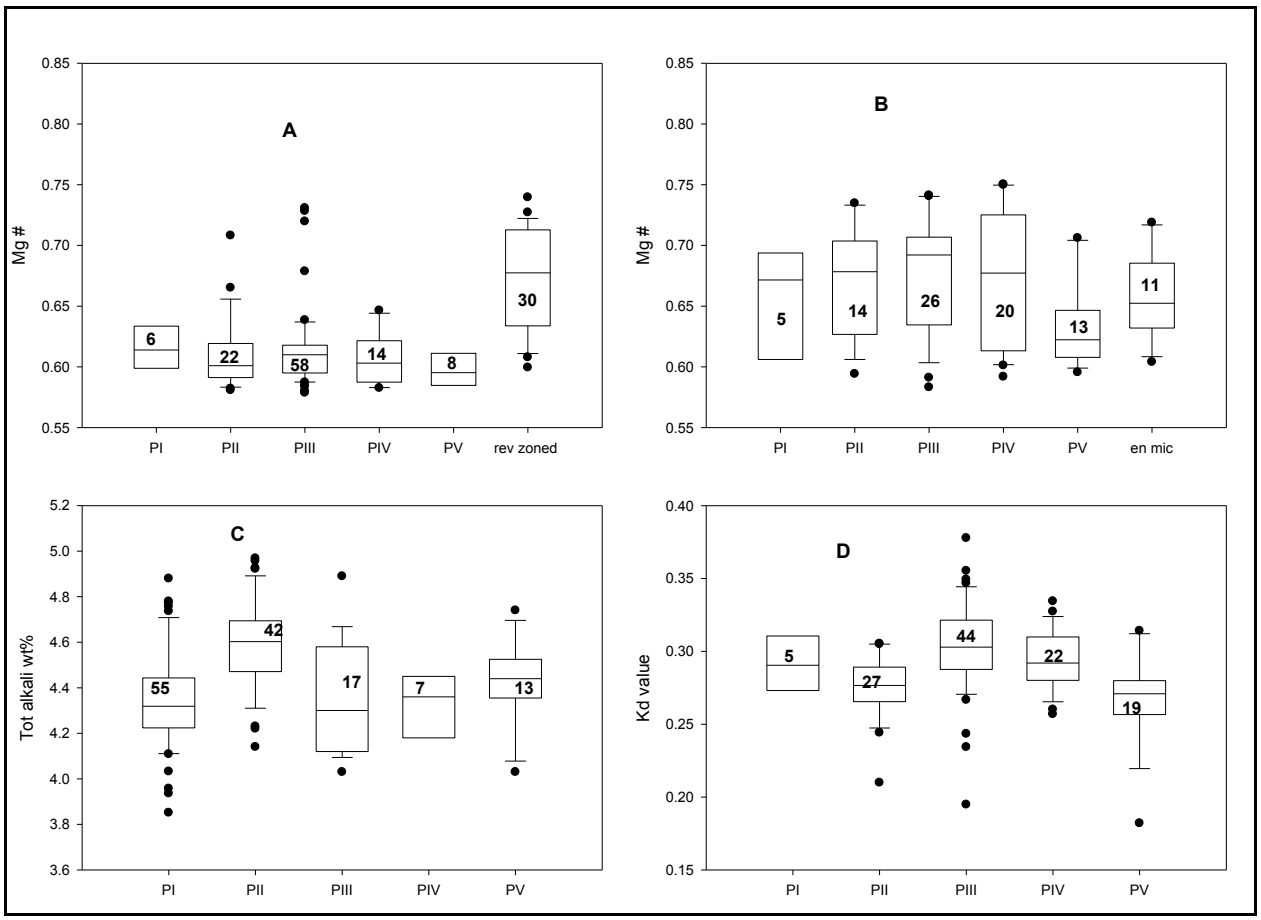

Figure 5 Box plots of mg# for andesite orthopyroxene unzoned rims (by phase) and rev-zoned rims A, andesite orthopyroxene microlites (by phase) and enclave microlites B, bulk rock total alkali by eruption phase C, andesite hosted clinopyroxene microlite Kd values by phase D. The number of analyses used is given in each box, horizontal line represents median values. an – andesites, en- enclaves.

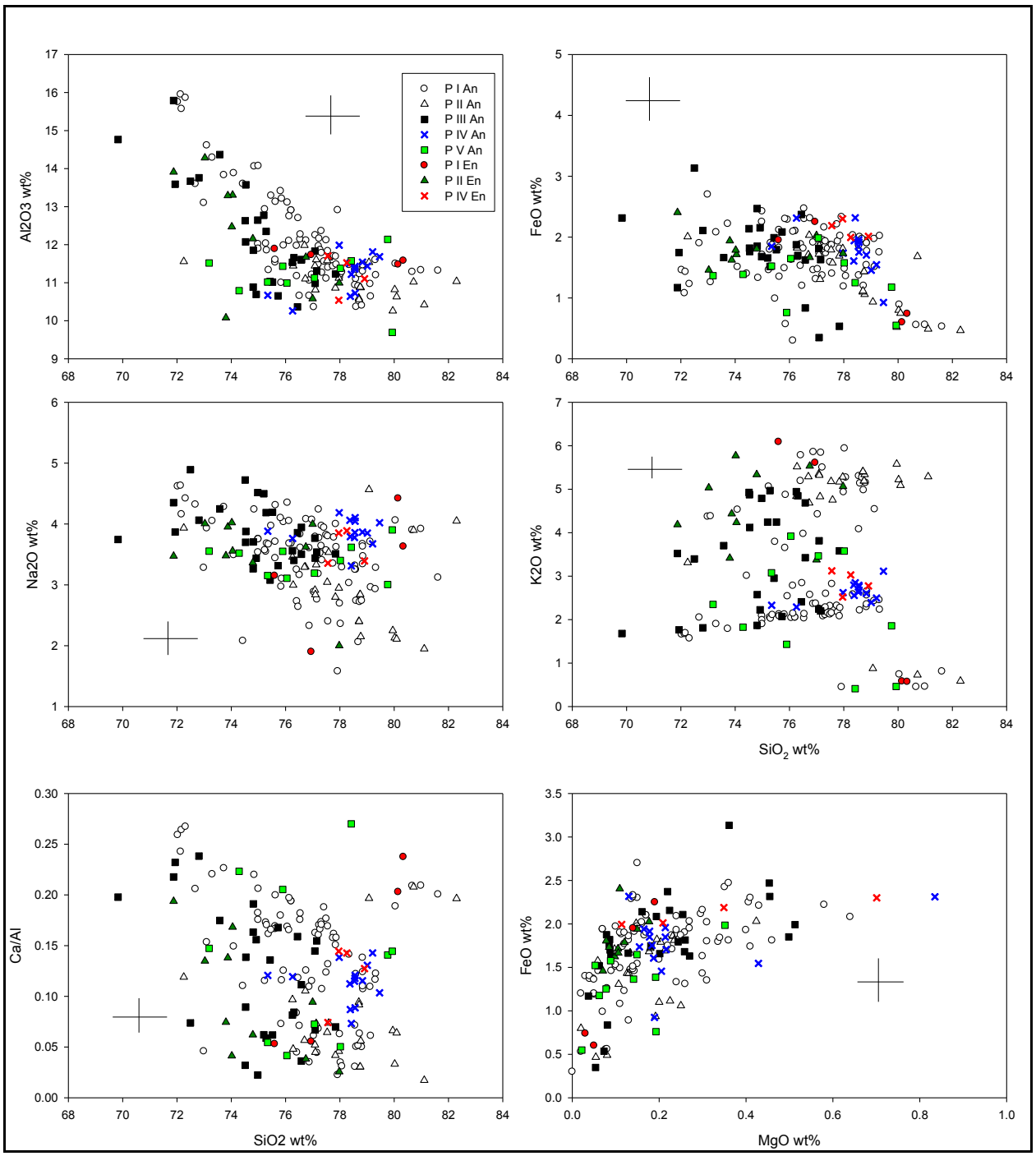

Figure 6 Abundances of major elements in andesite and enclave glass from microprobe analyses, andesites- An, enclaves- En. High K_2O > 3wt%, low K_2O < 3wt%.

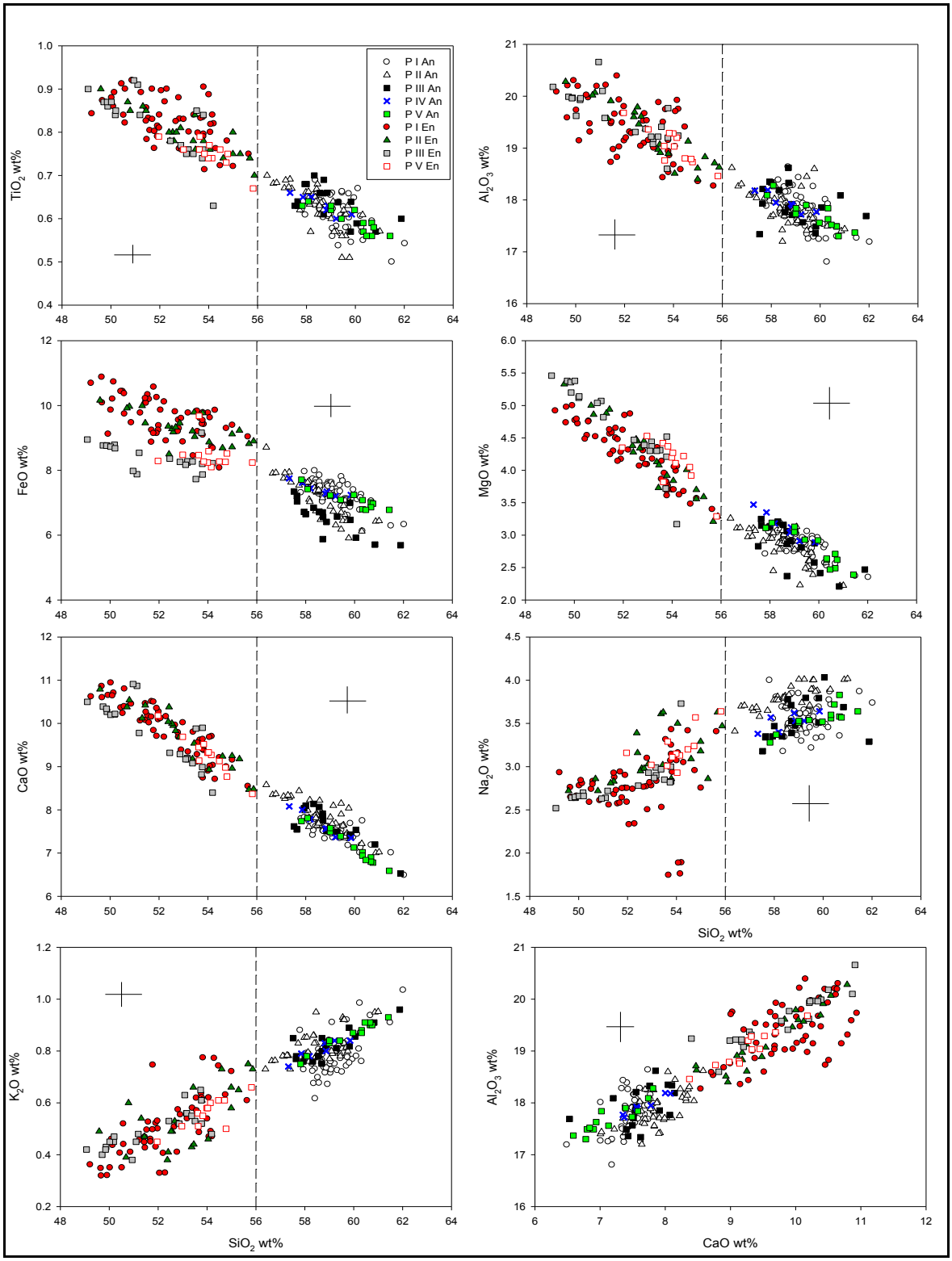

Figure 7 Bulk andesite and enclave major element abundances by phase, vertical dashed line demarcates boundary between silica content of the andesite- An, enclave- En.

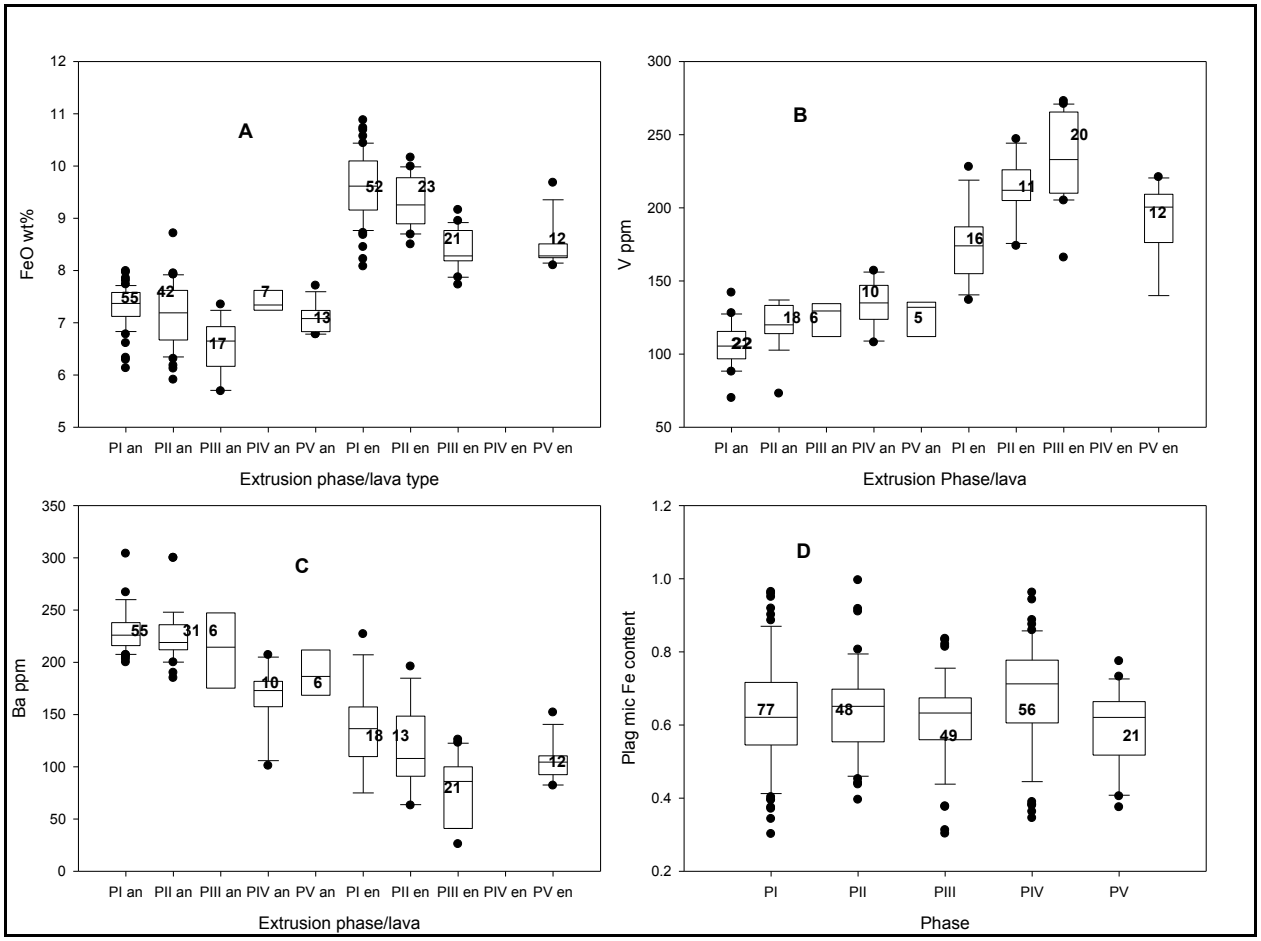

Figure 8 Box plots showing inter-phase bulk rock contents of FeO, V, Ba and plagioclase microlite Fe content throughout the eruption. The number of analyses used is given in each box, horizontal line represents median values, mic- microlite, an – andesites, en- enclaves.

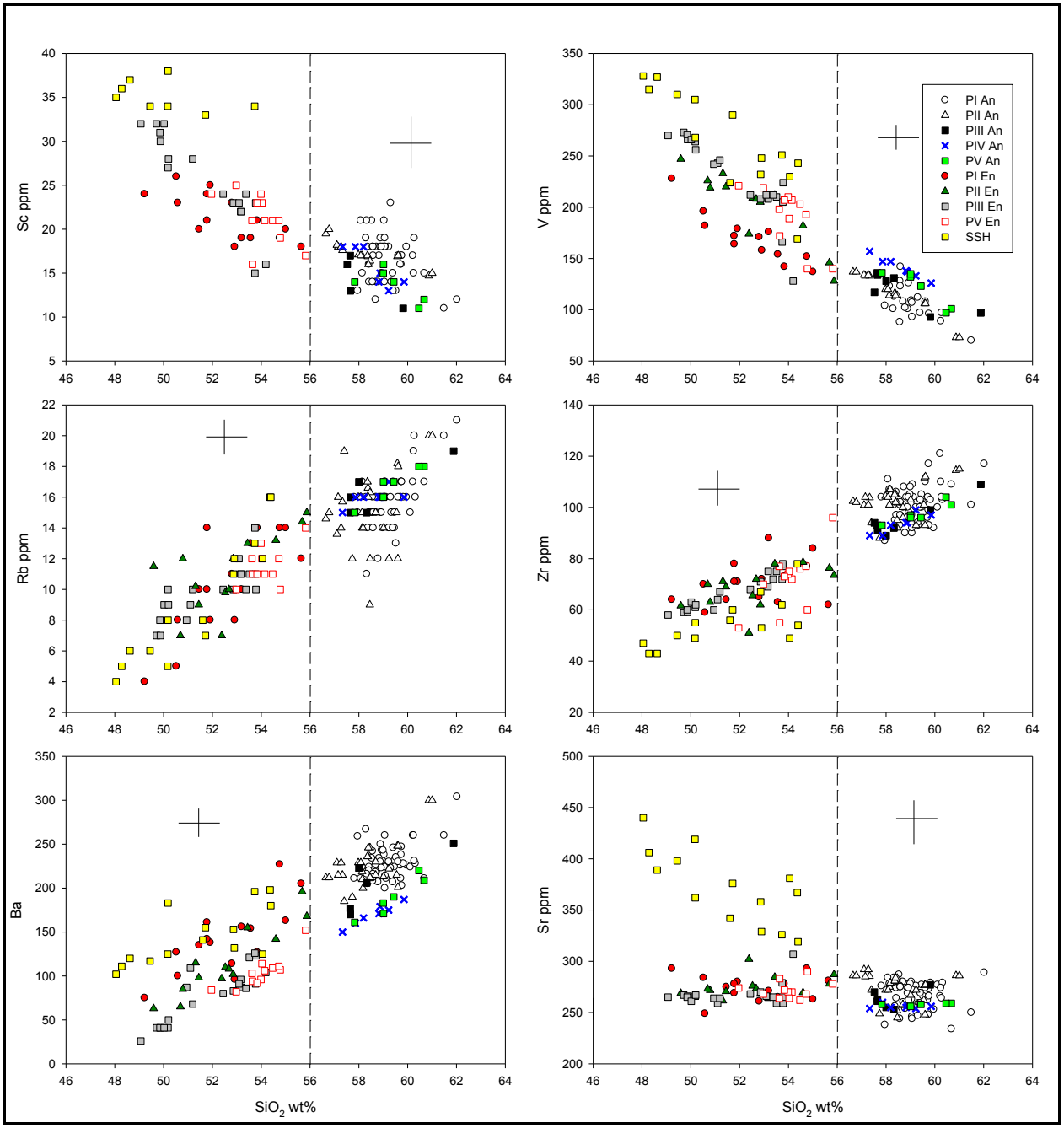

Figure 9 Selected trace element plots for bulk rock andesite and enclave products. Symbols and labels are the same as Figure 7, vertical line demarcates boundary between andesite and enclave silica content.

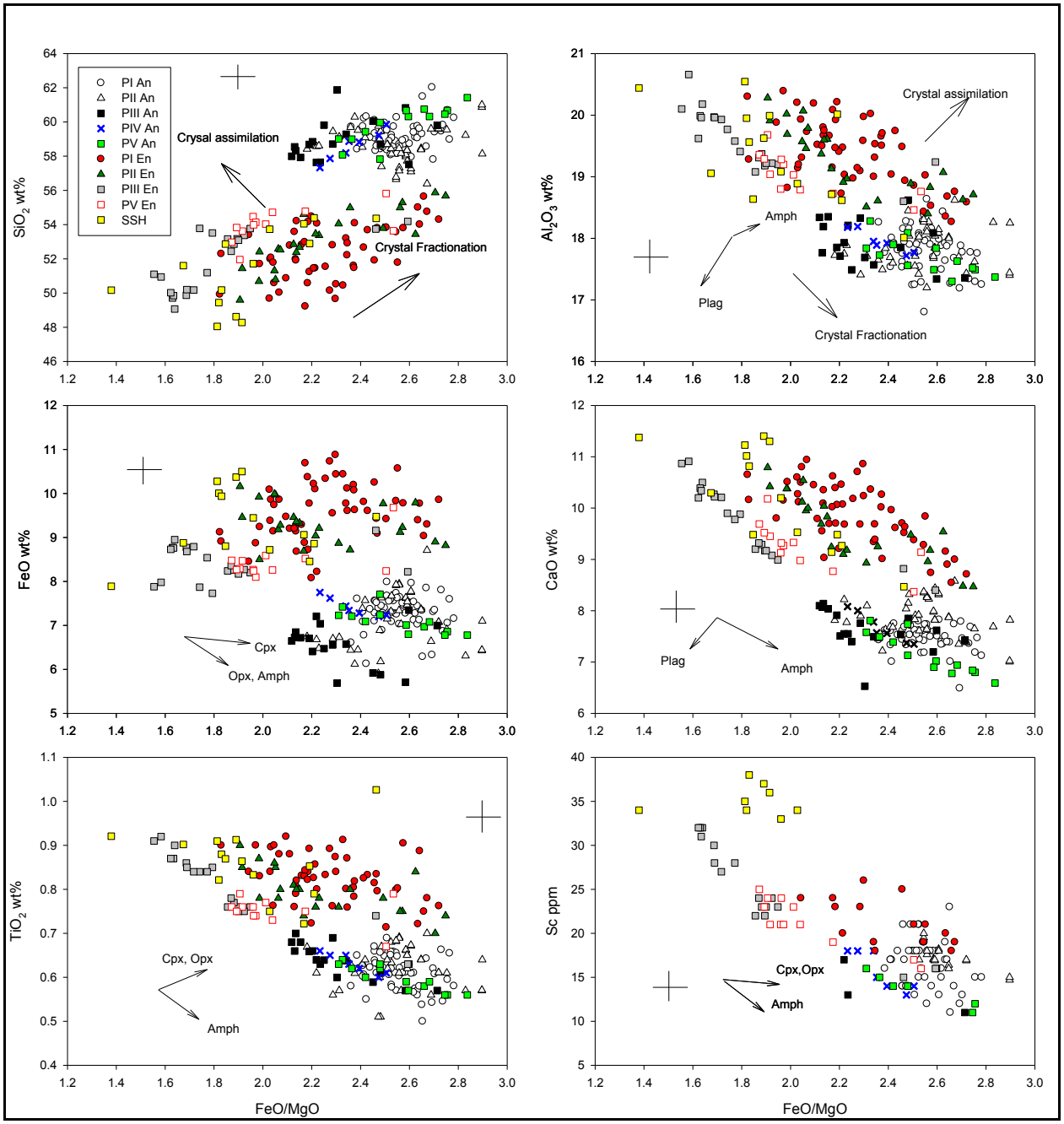

Figure 10 Major element behaviour with changing FeO/MgO showing changes as function of crystal control. Arrows indicate removal of particular mineral phase. An- andesite, En – enclaves. Fractionation and assimilation vectors for the other oxides are same as in Al_2O_3.

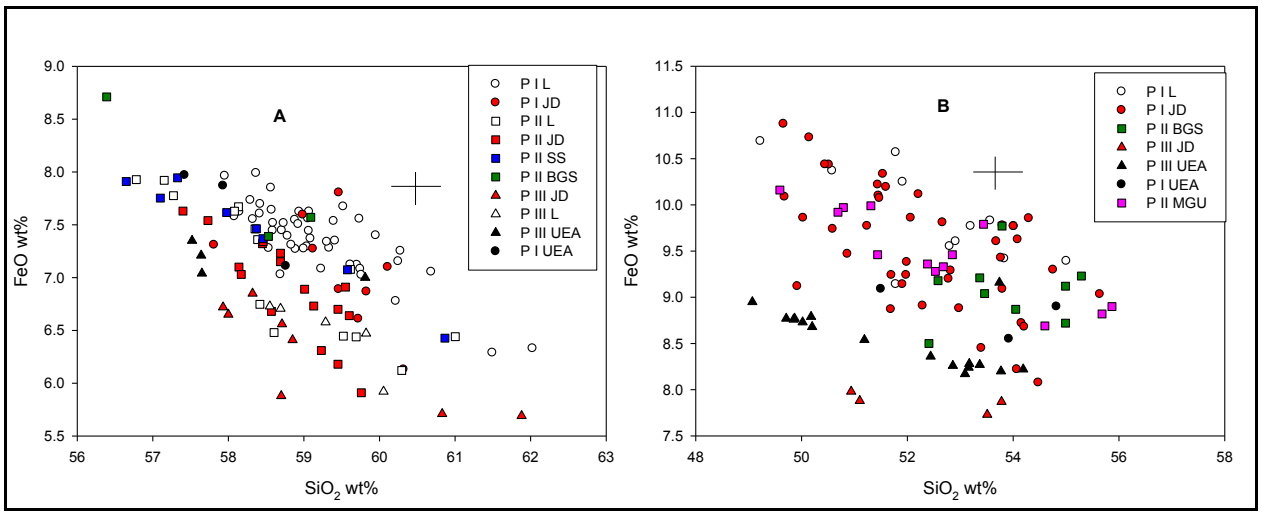

Figure 11 Harker plots of SiO_2 vs FeO for phases 1, II and III by lab showing an absence of any systematic inter-lab variation in the data for andesites- A and enclaves-B. L-leciester, JD- Joe Devine, SS- (Murphy et al., 1998), BGS- British geological survey, UEA- University of East Anglia, MGU- Mc Gill University.

Lab/Location	Instrument	Samples analyzed by Lab		Phase	Total Number of samples
		An	**En**		
University of East Anglia	Brucker-AXS S4 Pioneer **F**luorescenceS spectrometer	1523,1524 M003, M010	M001& M002 M004 to M009 M011 to M019	III	An - 4 En - 17
		1532,1535		IV	An -7
		1537 to 1544	1542, 1566 (a to e) 1587 to 1593	V	An - 12
McGill University, Canada	Philips PW2440 4 kW automated XRF		CM 36 to 38	I	En -3
			CM (26,28,41,51,52,56,58,62,64,65,66,75 A,77)	II	En -13
BGS labs	Spectron X-LAB 2000 ED-XRF	1247/AND (1 to 3)	MVO 1247/MI (1 to 8b)	II	An – 3 En - 9
University of Leicester	PANalytical Axios Advanced PW4400 XRF	40,45 to 57,174 to 242,244 to 332,665 to 725,1003 to 1091	36,49,60 to 63,107 to 115, 663, 675, 679, 682, 1133	I	An – 46 En - 11
		1151,1209 to 1217		II	An - 21
		1323,1330,1350,1387,1445 to 1448		III	An -7
Brown University		94 ,160,171,243	60 to 63, 163 to 165, 488, 530 to 532, 545,551,558, 560 to 564,570 to 572, 580,589	I	An -9 En - 41
		1151A, 1175, 1206, 1208 to1218		II	An - 19
		1323 to 1325, 1327, 1350,1387	1325 (a & b), 1326 (a & b)	III	An – 9 En 4

Table 1 Laboratory and sample information for the XRF data used in this study; An-andesite, En- enclave.

Phase	Total	Plagioclase	Amphibole	Opx	Ti-mag	Qtz	cpx
Murphy et al., 2000 Phase I	45-55	30-35	6-10	2-5	2-4	<0.5	0.5
Murphy et al., 2000 Phase I enclaves		1-5% + xenos	'xenos'	'xenos'		'xenos'	
Devine et al, 1998 Phase I	~40	~30	<6.5	<5	<2	rare	g.mass
Humphreys et al., 2009a*, Phase III	55-63	20-32	3-9.2	1.5-3	0.57-2.58	0-0.76	0.27-1.46
Humphreys et al.,2009a Phase II	33-42	26-32	5-7.5	1.5-3	0.76-1.39	0.05-0.4	0.5-0.66

Table 2 Published modal mineral contents for the first three extrusion phases. Arbitrary distinction between microlites and microphenocryst defined by 100μm, *Recalculated from point counts in Humphreys et al.,2009a, range shown.

Mineral Phase	Crystal Textures Present	
	Andesite	**Enclave**
Plagioclase	subhedral –euhedral phenocrysts, zoning (sieved, normal, reverse, patchy and oscillatory) normally zoned microlites euhedral, hopper shaped or skeletal	subhedral-euhedral phenocrysts zoning (sieved, normal, reverse and oscillatory); interpreted as inherited phenocrysts from the andesite euhedral microphenocrysts microlites (euhedral, dendritic, acicular or hopper shaped)
Amphibole	anhedral –euhedral phenocrysts rims (decompression, thermal and resorbed) rare microlites present in phase II	euhedral-subhedral microphenocrysts euhedral microlites Large inherited phenocrysts typically have thermal breakdown textures
Orthopyroxene	euhedral-subhedral phenocrysts zoning (normal, reverse) skeletal microlites	euhedral-anhedral microphenocrysts Large inherited phenocrysts typically have cpx overgrowth rims
Clinopyroxene	euhedral-subhedral microphenocrysts, zoning (normal; rare oscillatory and sector) skeletal, normally zoned microlites	subhedral-euhedral microphenocrysts overgrowths on amphibole rims
Fe-Ti oxides	euhedral-subhedral, unzoned phenocryst anhedral –subhedral, zoned microphenocrysts euhedral microlites	euhedral microphenocrysts euhedral-subhedral microlites
Quartz	Rounded and embayed, sometimes with cpx overgrowth rim	Rounded and embayed with cpx overgrowth rim

Table 3 Mineral phases and associated textures in the andesite and enclave lavas of the current eruption.

Description	PI-PIII pc	PV pc	PI-PIII pr	PIV pr	PV pr	PI-PIII mc	PIV mc	PV mc	PI-PIII mr	PIV mr	mpc	mpr	mr
Host	**An**	**An**	**An**	**An**	**An**	**An**	**An**	**An**	**An**	**An**	**En**	**En**	**En**
n	**35**	**20**	**71**	**64**	**14**	**89**	**35**	**38**	**32**	**19**	**23**	**26**	**25**
SiO2	53.15	55.28	53.54	53.5	54.5	51.12	51.04	49.62	52.9	51.21	47.94	51.65	49.26
TiO2	0.01	0.02	0.02	0.02	0.01	0.02	0.03	0.03	0.02	0.03	0.02	0.03	0.02
Al2O3	29.4	28.8	28.5	28.9	29	30	30.8	31.62	28.7	30.24	31.92	29.51	31.2
FeO	0.4	0.28	0.5	0.5	0.3	0.64	0.7	0.7	0.6	0.7	0.64	0.66	0.68
MgO	0.04	0.02	0.07	0.08	0.02	0.08	0.08	0.18	0.09	0.07	1.47	0.08	0.08
CaO	12.63	11.27	12	11.8	11.41	13.6	13.8	14.73	12.19	13.6	14.85	13.26	15.1
Na2O	4.4	4.94	4.47	4.72	4.9	3.64	3.6	3	4.42	3.7	2.13	3.87	2.91
K2O	0.14	0.12	0.16	0.15	0.11	0.11	0.12	0.07	0.12	0.18	0.05	0.12	0.09
Total	100.18	100.72	99.21	99.62	100.18	99.17	100.08	99.86	98.99	99.73	99.02	99.18	99.34
Mean XAn	60.5	55	58.8	57.1	55.6	66.6	67.1	72.71	59.63	66.11	79	64.7	74.2
± 1σ	11	4	10	8	5	8	10	9	7	9	9	9	11

Table 4 Averaged andesite plagioclase phenocryst and microlite microprobe data, comparing compositions from Phases IV and V with the published compositions of Phases I, II and III. pc- phenocryst core, pr - phenocryst rim, mc- microlite core, mr- microlite rim, mpc- microphenocryst core, mpr – microphenocryst rim, An- andesite, En – enclave.

	P1-P3 phx core	P5 core	P1-P3 phx rim	P4 rim	P5 rim	P1-P3 mphx core	P4 mphx core	P5 mphx core
n	**108**	**27**	**32**	**7**	**14**	**13**	**4**	**14**
SiO2	47.29	47.14	47.35	47.43	47.35	45.06	48.2	45.7
TiO2	1.46	1.46	1.44	1.44	1.41	1.63	1.46	1.64
Al2O3	7.11	7.32	7.15	7.37	6.94	9.56	6.79	8.36
FeO	14.78	14.91	14.4	14.72	14.61	13.88	14.63	15.5
MnO	0.53	0.51	0.5	0.51	0.53	0.39	0.54	0.48
MgO	13.64	13.69	13.85	13.81	13.8	13.68	13.78	12.96
CaO	10.7	10.71	10.79	10.95	10.79	10.74	10.84	10.72
Na2O	1.36	1.36	1.34	1.36	1.3	1.73	1.26	1.55
K2O	0.19	0.19	0.19	0.2	0.19	0.21	0.17	0.22
Cl	0.11	0.14	0.12	0.13	0.14	0.11	0.13	0.17
Total	97.17	97.42	97.12	97.91	97.06	96.98	97.8	97.3
Mg #	**0.48±0.02**	**0.48±0.02**	**0.49±0.03**	**0.48±0.03**	**0.49±0.02**	**0.50±0.05**	**0.49±0.01**	**0.46±0.02**

Table 5a Averaged andesite amphibole compositions by texture and eruption phase.

	P1 en		P2 en		P3 en		P5 en	Mph		Frag	
n	16	± 1σ	11	± 1σ	8	± 1σ	36	9	± 1σ	19	± 1σ
SiO2	42.07	1.75	41.91	1.43	41.15	0.8	41.35	41.69	1.15	42.1	1.34
TiO2	1.74	0.16	1.94	0.13	1.94	0.09	2.00	1.83	0.15	1.92	0.14
Al2O3	12.92	2.12	13.26	1.8	14.16	0.7	14.49	13.5	1.33	12.88	1.63
FeO	13.09	1.37	11.7	1.14	10.28	0.8	10.30	11.89	1.78	11.84	1.43
MnO	0.28	0.16	0.19	0.08	0.15	0.02	0.13	13.77	0.91	14.04	0.78
MgO	13.17	0.92	13.96	0.76	14.81	0.46	15.00	0.2	0.06	0.21	0.09
CaO	11.53	0.32	11.33	0.36	11.62	0.19	11.85	11.2	0.4	11.1	0.52
Na2O	2.21	0.2	2.21	0.21	2.41	0.04	2.42	2.25	0.2	2.22	0.23
K2O	0.2	0.04	0.22	0.02	0.21	0.02	0.25	0.24	0.02	0.21	0.02
Cl	-	-	0.07	0.05	0.05	0.03	0.02	0.06	0.03	0.04	0.03
Tot	97.19		96.79		96.78		97.80	96.63		96.56	
Mg#	**0.5**	**0.04**	**0.54**	**0.03**	**0.59**	**0.03**	**0.59**	**0.54**	**0.05**	**0.54**	**0.04**

Table 5b Averaged enclave amphibole compositions from eruption Phases I, II, III and V along side high aluminum andesite hosted microphenocrysts and groundmass fragments. Mphx – microphenocrysts, Frag – groundmass fragments. Phase V data from Plail et al. (this volume)

	P1-P3 phx core	P5 phx core	P1-P3 phx rim	P4 phx rim	P5 phx rim	P1-P3 mic core	P4 mic core	P5 mic core
n	**106**	**15**	**72**	**13**	**8**	**38**	**19**	**12**
SiO2	52.37	52.43	52.45	52.44	52.65	52.92	52.7	53.26
TiO2	0.11	0.11	0.12	0.11	0.12	0.2	0.21	0.17
Al2O3	0.59	0.58	0.69	0.64	0.62	1.41	1.24	1.05
FeO	24.18	24.19	23.17	23.68	24.21	19.68	19.92	21.8
MnO	1.57	1.58	1.48	1.53	1.66	0.92	0.97	1.27
MgO	20.08	20	20.61	20.3	20.14	22.67	22.93	21.17
CaO	1	0.95	1.06	1.01	1.02	1.6	1.6	1.3
Na2O	0.01	0.02	0.01	0.02	0.02	0.03	0.04	0.02
Tot	99.93	99.85	99.6	99.72	100.43	99.43	99.61	100.01
En	**58.82**	**59**	**60.29**	**59.84**	**58.82**	**65.34**	**65.95**	**62.15**
Fs	**39.07**	**39**	**37.47**	**37.86**	**39.05**	**31.34**	**30.75**	**35.15**
Mg#	**0.6 ± 0.02**	**0.6 ±0.01**	**0.61 ±0.03**	**0.61 ± 0.02**	**0.6 ±0.01**	**0.67 ±0.05**	**0.67 ±0.06**	**0.63 ±0.04**

Table 6a Averaged Orthopyroxene phenocryst and microlite compositions comparing the andesite crystals of phase IV and V with crystals from phases I, II and III , errors are ± 1σ, mic – microlites, phx-phenocrysts.

	Opx-Mphx core	Opx-Mphx rim	Rev zoned Opx-Phx rims	Opx Mphx
Host	**Andesite**	**Andesite**	**Andesite**	**Enclave**
n	**12**	**15**	**18**	**18**
SiO_2	52.43	52.5	53.35	52.5
TiO_2	0.11	0.16	0.16	0.23
Al_2O_3	0.65	0.86	1.04	1.33
FeO	23.28	22.55	19.82	21.18
MnO	1.48	1.4	0.93	1.08
MgO	20.35	20.77	23.15	22.02
CaO	0.98	1.23	1.5	1.48
Na_2O	0.01	0.02	0.02	0.03
Tot	99.3	99.48	99.98	99.84
En	**59.7**	**60.7**	**65.9**	**63.6**
Fs	**38.2**	**36.8**	**31**	**33.3**
Mg#	**0.61 ± 0.02**	**0.62 ± 0.03**	**0.7 ± 0.02**	**0.64 ± 0.05**

Table 6b Averaged compositions of andesite hosted reverse zoned orthopyroxene phenocryst rims along with andesite and enclave microphenocrysts, errors are ± 1σ , Mphx- microphenocrysts, Phx- phenocrysts.

	P1-P3 Andesite mphx	P5 Andesite mphx	P1-P3 Andesite mic	P4 Andesite mic	P5 Andesite mic	Andesite hosted overgrowths	Enclave mphx
n	**29**	**8**	**66**	**23**	**18**	**28**	**24**
SiO2	51.22	52.22	51.22	50.71	50.85	50.25	50.5
TiO2	0.45	0.32	0.5	0.63	0.53	0.6	0.62
Al2O3	2.28	1.61	2.88	3.04	2.91	3.61	3.26
FeO	10.51	9.99	10.19	10.18	9.88	9.66	10.83
MnO	0.54	0.63	0.49	0.44	0.47	0.38	0.52
MgO	14.8	14.66	14.53	14.47	14.51	14.49	14.22
CaO	19.06	20.4	18.93	19.65	19.74	19.62	18.99
Na2O	0.23	0.22	0.24	0.27	0.28	0.23	0.27
Total	99.08	100.05	98.97	99.37	99.17	98.84	99.21
Si/Al	22.46	32.43	17.78	16.68	17.47	13.92	15.49
Wo	**40.72**	**42.8**	**40.75**	**42.56**	**42.73**	**42.6**	**41.3**
En	**43.93**	**42.8**	**43.52**	**43.58**	**43.7**	**43.7**	**43.1**
Mg#	**0.72 ±0.01**	**0.72 ± 0.03**	**0.72 ± 0.02**	**0.72 ± 0.02**	**0.72 ± 0.03**	**0.72 ±0.03**	**0.7 ± 0.02**

Table 6c Averaged compositions of clinopyroxene microphenocrysts, microlites and overgrowths, errors are ± 1σ, mic – microlites, mphx- microphenocrysts.

	P1-P3 mph cores	P4 mph cores	P5 mph cores	P1-P3 mph rims	P4 mph rims	P5 mph rims	P1-P3 mic	P4 mic	P5 mic
n	**32**	**9**	**9**	**21**	**15**	**8**	**69**	**27**	**5**
SiO2	0.09	0.12	0.11	0.11	0.13	0.1	0.38	0.54	0.3
TiO2	8.4	10.26	8.11	8.27	9.64	8.03	10.69	10.8	7.71
Al2O3	2.04	1.67	1.97	2.19	1.76	1.72	2.02	1.82	1.83
FeO	80.85	81.17	82.27	80.94	81.06	81.98	77.55	79.1	80.6
MnO	0.62	0.58	0.63	0.6	0.62	0.59	0.62	0.67	0.63
MgO	1.27	1.32	1.18	1.16	1.39	1.26	1.15	1.38	1.08
CaO	0.04	0.03	0.04	0.04	0.16	0.08	0.1	0.15	0.09
Total	93.31	95.15	94.32	93.3	94.75	93.77	92.5	94.46	92.23
Usp mol%	**25**	**30**	**24**	**25**	**28**	**23**	**33**	**32**	**23**
± 1σ	5	6	2	4	6	1	9	5	1

Table 7a Averaged andesite titanomagnetite compositions, sorted by eruptive phase and textural type. Usp/Ilm mol% after Stormer (1983), mic – microlites.

	En Mic	En mph	An Ilm	En Ilm
n	**22**	**12**	**26**	**8**
SiO2	0.39	0.15	0.03	0.03
TiO2	11.99	8.46	42.4	43.5
Al2O3	1.73	2.44	0.2	0.21
FeO	77.49	81.45	51.15	50.1
MnO	0.57	0.59	0.79	0.78
MgO	1.15	1.26	2.19	2.04
CaO	0.13	0.06	0.05	0.05
Total	93.45	94.4	96.81	96.68
Usp/Ilm mol %	**36**	**28**	**80**	**83**
± 1σ	11	8	3	6

Table 7b Averaged compositions of enclave oxides along with andesite hosted ilmenite.

Andesite	**n**	**SiO2**	**TiO2**	**Al2O3**	**FeO**	**MgO**	**CaO**	**Na2O**	**K2O**	**Total**	**Mg#**	**Fe/Mg**	**Ca/Al**	**Tot alkali**	***fO2 logunits***
Phase 1	**81**	76.64	0.37	12.15	1.72	0.23	1.81	3.51	2.84	99.34	0.1	7.5	0.14	6.35	NNO +1- +1.2
± *σ*		***2.2***	***0.09***	***1.3***	***0.5***	***0.26***	***1***	***0.6***	***1.4***	***1.1***	***0.07***		***0.07***	***1.2***	
Phase 2	**21**	78.22	0.4	11.09	1.37	0.17	0.89	3	4.56	99.6	0.1	8	0.08	7.56	NNO + 0.5- +1.3
± *σ*		***2***	***0.19***	***0.45***	***0.5***	***0.09***	***0.6***	***0.7***	***1.5***	***1.2***	***0.05***		***0.05***	***1.1***	
Phase 3	**40**	75.71	0.35	11.64	1.8	0.2	1.28	3.77	3.85	98.9	0.1	9	0.11	7.7	NNO+ 0.5- +1.4
± *σ*		***2.2***	***0.14***	***1.45***	***0.6***	***0.14***	***0.9***	***0.7***	***1.3***	***1.3***	***0.05***		***0.06***	***1.3***	
Phase 4	**14**	78.25	0.3	11.26	1.78	0.25	1.28	3.87	2.64	99.8	0.12	7	0.11	6.5	NNO+ 0.9- +1.1
± *σ*		***1.12***	***0.12***	***0.5***	***0.4***	***0.18***	***0.3***	***0.2***	***0.2***	***1.4***	***0.06***		***0.02***	***0.3***	
Phase 5	**13**	76.09	0.27	11.8	1.34	0.14	1.46	3.04	2.44	97	0.1	9.6	0.12	5.5	NNO +1.4
± *σ*		***2***	***0.07***	***1.4***	***0.3***	***0.1***	***0.9***	***0.6***	***0.8***	***2.2***	***0.05***		***0.06***	***1***	
Enclave															
Phase 1	**4**	78.26	0.44	11.67	1.39	0.1	1.59	3.28	3.21	100.01	0.07	13.9	0.14	6.5	
± *σ*		***2.4***	***0.12***	***0.18***	***0.8***	***0.08***	***1.11***	***1.06***	***3.1***	***0.01***	***0.02***		***0.1***	***2.3***	
Phase 2	**10**	74.7	0.41	12.3	1.8	0.11	1.24	3.6	4.6	98.9	0.06	16.6	0.1	8.19	
± *σ*		***1.9***	***0.1***	***1.4***	***0.26***	***0.03***	***0.9***	***0.6***	***0.8***	***1.7***	***0.01***		***0.06***	***0.98***	
Phase 4	**4**	78.17	0.4	11.22	2.12	0.34	1.36	3.62	2.9	100.3	0.13	6.2	0.12	6.5	
± *σ*		***0.6***	***0.19***	***0.5***	***0.15***	***0.26***	***0.3***	***0.3***	***0.3***	***0.4***	***0.08***		***0.03***	***0.32***	

Table 8 Averaged microprobe glass compositions for andesites and enclaves, along with log *f*o2 values from touching ilmenite–magnetite pairs.

Andesite	n	SiO2	TiO2	Al2O3	FeO	MnO	MgO	CaO	Na2O	K2O	P2O5	Tot	Fe/Mg	Ca/Al	Tot alk
Phase 1	**55**	59.22	0.61	17.81	7.32	0.18	2.87	7.49	3.56	0.78	0.15	99.99	2.56	0.42	4.35
± σ		***0.82***	***0.04***	***0.36***	***0.39***	***0.02***	***0.19***	***0.24***	***0.18***	***0.08***	***0.01***	***0.1***	***0.1***	***0.01***	***0.22***
Phase 2	**42**	58.6	0.63	17.86	7.14	0.18	2.81	7.87	3.77	0.82	0.16	99.83	2.55	0.44	4.59
± σ		***1.07***	***0.05***	***0.35***	***0.61***	***0.02***	***0.27***	***0.38***	***0.16***	***0.06***	***0.01***	***0.32***	***0.17***	***0.02***	***0.19***
Phase 3	**17**	58.96	0.64	17.92	6.56	0.17	2.85	7.63	3.53	0.82	0.14	99.19	2.32	0.43	4.35
± σ		***1.2***	***0.04***	***0.38***	***0.5***	***0.02***	***0.33***	***0.4***	***0.23***	***0.06***	***0.02***	***0.61***	***0.18***	***0.02***	***0.24***
Phase 4	**7**	58.59	0.63	17.95	7.41	0.18	3.14	7.67	3.52	0.8	0.14	100.03	2.37	0.43	4.33
± σ		***0.86***	***0.02***	***0.18***	***0.21***	***0.01***	***0.22***	***0.29***	***0.1***	***0.04***	***-***	***0.31***	***0.10***	***0.01***	***0.13***
Phase 5	**13**	59.91	0.59	17.68	7.08	0.18	2.76	7.12	3.56	0.86	0.14	99.81	2.58	0.4	4.42
± σ		***1.11***	***0.03***	***0.3***	***0.28***	***-***	***0.27***	***0.4***	***0.14***	***0.06***	***0.01***	***0.18***	***0.16***	***0.02***	***0.19***
Enclave															
Phase 1	**55**	52.36	0.84	19.38	9.61	0.2	4.26	9.88	2.76	0.51	0.14	99.95	2.27	0.51	3.27
± σ		***1.57***	***0.08***	***0.54***	***0.63***	***0.02***	***0.43***	***0.6***	***0.36***	***0.12***	***0.02***	***0.23***	***0.22***	***0.03***	***0.42***
Phase 2	**22**	53.13	0.8	19.27	9.31	0.21	4.2	9.63	3.12	0.55	0.13	100.34	2.25	0.5	3.66
± σ		***1.71***	***0.05***	***0.56***	***0.47***	***0.02***	***0.58***	***0.66***	***0.3***	***0.11***	***0.02***	***0.35***	***0.26***	***0.02***	***0.33***
Phase 3	**22**	51.89	0.81	19.59	8.44	0.18	4.68	9.77	2.82	0.5	0.11	98.7	1.83	0.5	3.32
± σ		***1.68***	***0.07***	***0.47***	***0.4***	***0.01***	***0.58***	***0.69***	***0.25***	***0.07***	***0.02***	***0.66***	***0.26***	***0.03***	***0.29***
Phase 5	**12**	54	0.75	19.04	8.45	0.18	4.13	9.26	3.2	0.56	0.12	99.69	2.06	0.49	3.76
± σ		***0.96***	***0.03***	***0.34***	***0.41***	***0.02***	***0.34***	***0.46***	***0.21***	***0.06***	***0.02***	***0.23***	***0.23***	***0.02***	***0.23***

Table 9 Averaged bulk rock major element compositions for the andesite and enclaves of the different eruption phases.

Andesite	n	Sc	V	Rb	Sr	Y	Zr	Ba	Zr/Rb	Zr/Ba	Zr/Ti	Ba/Rb	Ba/K
Phase 1	**55**	16.61	106.23	15.23	272.37	24.31	101.57	225.16	6.8	0.45	161.77	15.04	273.18
± σ		**2.71**	**15.84**	***2.42***	***14.11***	***1.37***	***6.66***	***25.44***	***0.97***	***0.03***	***16.21***	***2.19***	***21.95***
Phase 2	**31**	17.19	117.58	15.23	272.37	24.31	101.57	225.16	6.8	0.45	161.77	15.04	273.18
± σ		**1.35**	**18.7**	***2.42***	***14.11***	***1.37***	***6.66***	***25.44***	***0.97***	***0.03***	***16.21***	***2.19***	***21.95***
Phase 3	**6**	14.25	115.63	16.83	261.5	21.33	97.13	212.17	5.8	0.46	145.83	12.57	251.19
± σ		***2.75***	***19.68***	***1.83***	***8.38***	***1.21***	***8.17***	***34.13***	***0.35***	***0.05***	***15.62***	***1.15***	***32.45***
Phase 4	**10**	15.71	140.71	16	255.86	20.86	93.57	169.71	5.85	0.55	148.53	10.6	211.25
± σ		***2.21***	***10.34***	***0.58***	***2.12***	***0.9***	***3.74***	***12.32***	***0.15***	***0.03***	***11.13***	***0.63***	***8.88***
Phase 5	**6**	13.20	117.8	16.8	258.2	21.4	98.2	192.6	5.86	0.51	168.42	11.44	226.55
± σ		***1.64***	***17.85***	***1.3***	***0.84***	***0.55***	***4.32***	***23.01***	***0.26***	***0.04***	***17.75***	***0.64***	***10.24***
Enclave													
Phase 1	**18**	21.33	174.88	10.61	275.22	23.04	69.56	136.78	7.42	0.55	88.45	13.68	247.66
± σ		***2.64***	***24.64***	***3.42***	***11.95***	***2.25***	***8.45***	***39.84***	***3.18***	***0.15***	***13.57***	***4.28***	***66.31***
Phase 2	**13**		200.69	11.08	275.74	22.66	68.59	115.69	6.44	0.65	85.1	10.45	204.53
± σ			***34.33***	***2.54***	***10.45***	***4.47***	***7.82***	***39.43***	***1.42***	***0.2***	***13.63***	***2.37***	***39.99***
Phase 3	**21**	25.41	227.77	9.84	267.24	20.43	63.14	77.76	6.69	0.97	77.85	7.92	153.4
± σ		***5.24***	***36.54***	***1.71***	***10.06***	***1.83***	***14.87***	***30.95***	***1.66***	***0.49***	***19.94***	***2.43***	***54.68***
Phase 5	**12**	21.25	191.58	11.55	271.92	22.33	71.50	104.17	6.34	0.69	95.91	9.18	185.56
± σ		***2.8***	***27.5***	***1.21***	***8.27***	***4.85***	***11.49***	***18.3***	***0.59***	***0.09***	***19.53***	***1.08***	***20.06***

Table 10 Averaged bulk rock trace element for andesites and enclaves of the different eruption phases.

Tmin °C	Tmax °C	Avg °C	Stdev ± °C	no. analyses	Method	Phase texture
824	965	866	30	17	Single-pyroxene QUILF method	Opx/Microphenocryst cores
845	895	869	15	14	Single-pyroxene QUILF method	Opx/Microphenocryst rims
1018	1032	1025	6	4	Single-pyroxene QUILF method	Opx/Microphenocryst rims (showing heated textures)
785	938	851	23	77	Single-pyroxene QUILF method	Opx/Phenocryst cores
799	1028	878	65	65	Single-pyroxene QUILF method	Opx/Phenocryst rims
826	1101	988	82	26	Single-pyroxene QUILF method	Opx/Zoned phenocryst rims
903	1305	1070	106	16	Single-pyroxene QUILF method	Opx/Mafic inclusions
791	809			4	2-oxides QUILF (Andersen et al. 1993)	Ox/Included in minerals or in crystal clots
958	1017			3	2-oxides QUILF (Andersen et al. 1993)	Ox/Zoned microphenocrysts or microlites
1074	1196	1109	45	5	2-pyroxene QUILF (Andersen et al. 1993)	2Px/Mafic inclusion pairs
903	1142	1021	78	15	2-pyroxene QUILF (Andersen et al. 1993)	2Px/Microlite pairs
804	890	833	24	10	Hb-plag equilibria Holland & Blundy	Hb-plg Andesite pairs (using ed-ri thermometer, 200 MPa)
849	947	894	34	9	Hb-plag equilibria Holland & Blundy	Hb-plg Mafic inclusion pairs (using ed-ri thermometer, 200 MPa)
821	1100	920	70	36	Plag-melt	Andesite hosted microlites (XAn 0.45-0.84)
1097	1145	1110	35	19	Cpx-melt	Enclave microlites/microphenocryst rims

Table 11 Temperature and Pressure estimates for the eruptive products obtained using a number of different techniques.

Initial	Final	amph wt%	Plag wt%	Opx wt%	Cpx wt%	Ox wt%	R^2
Phase I Low Fe andesite	Phase I High Fe andesite	+11	-4	+10	-16	-4	0.15
Phase II Low Fe andesite	Phase II High Fe andesite	-	+16	+6	+3	+4	0.025
Phase III Low Fe andesite	Phase III High Fe andesite	-	+9	+1	+5	+3	0.25

Table 12 Intra- phase andesite mass balance calculations for addition of enclave crystals, weight % values are relative to initial magma compositions.